A Plague of Magnetic Spots Among the Hot Stars of Globular Clusters

Y. Momany[1], S. Zaggia[1], M. Montalto[2], D. Jones[3,4], H.M.J. Boffin[5], S. Cassisi[6,7], C. Moni Bidin[8], M. Gullieuszik[1], I. Saviane[9], L. Monaco[10], E. Mason[11], L. Girardi[1], V. D'Orazi[1], G. Piotto[2], A.P. Milone[2], H. Lala[2], P.B. Stetson[12] & Y. Beletsky[13]

[1] *INAF - Osservatorio Astronomico di Padova, Vic. dell'Osservatorio 5, 35122 Padova, Italy*

[2] *Dipartimento di Fisica e Astronomia, Univ. di Padova, V. dell'Osservatorio 3, 35122 Padova*

[3] *Instituto de Astrofisica de Canarias, E-38205 La Laguna, Tenerife, Spain*

[4] *Departamento de Astrofisica, Universidad de La Laguna, E-38206 La Laguna, Tenerife, Spain*

[5] *European Southern Observatory, Karl Schwarzschild Strasse 2, D-85748 Garching, Germany*

[6] *INAF - Osservatorio Astronomico d'Abruzzo, Via M. Maggini, I-64100 Teramo, Italy*

[7] *INFN - Sezione di Pisa, Largo Pontecorvo 3, 56127 Pisa, Italy*

[8] *Instituto de Astronomía, Universidad Católica del Norte, Av. Angamos 0610, Antofagasta, Chile*

[9] *European Southern Observatory, Alonso de Cordova 3107, Santiago, Chile*

[10] *Departamento de Ciencias Fisicas, Universidad Andres Bello, Fernandez Concha 700, Las Condes, Santiago, Chile*

[11] *INAF - Osservatorio Astronomico di Trieste, Via G.B. Tiepolo, 11, I-34143, Trieste, Italy*

[12] *Herzberg Astronomy and Astrophysics, National Research Council, 5071 West Saanich Road, Victoria, BC V9E 2E7, Canada*

[13] *Las Campanas Observatory, Carnegie Institution of Washington, Colina el Pino, Casilla 601, La Serena, Chile*

Six decades and counting, the formation of hot $\sim 20,000 - 30,000$ K Extreme Horizontal Branch (EHB) stars in Galactic Globular Clusters remains one of the most elusive quests in stellar evolutionary theory. Here we report on two discoveries shattering their currently alleged stable luminosity. The first EHB variability is periodic and cannot be ascribed to binary evolution nor pulsation. Instead, we here attribute it to the presence of magnetic spots: superficial chemical inhomogeneities whose projected rotation induces the variability. The second EHB variability is aperiodic and manifests itself on time-scales of years. In two cases, the six-year light curves display superflare events a mammoth several million times more energetic than solar analogs. We advocate a scenario where the two spectacular EHB variability phenomena are different manifestations of diffuse, dynamo-generated, *weak* magnetic fields. Ubiquitous magnetic fields, therefore, force an admittance into the intricate matrix governing the formation of all EHBs, and traverse to their Galactic field counterparts. The bigger picture is one where our conclusions bridge similar variability/magnetism phenomena in *all* radiative-enveloped stars: young main-sequence stars, old EHBs and defunct white dwarfs.

We report on the results of a monitoring survey of the hot stellar populations in three Globular Clusters (GCs). The novelty resides in exploiting the near-ultraviolet filters that suppress the contribution of the (undesired) bright/cool red giant stars and enhance that of the faint/hot stars – the targets of the survey. These are the $\sim 0.48 \, M_\odot$ stars spanning temperatures between $20,000 - 30,000$ K, referred[1] to as Extreme Horizontal Branch (EHB) stars when identified in

1

GCs (and sub-dwarf B-type, sdB, when found in the Galactic field). EHBs are believed to have lost $\sim 30\%$ of their original mass and almost the entirety of their envelope[2]. Their Hydrogen shell is so thin ($\lesssim 0.02\,\mathrm{M_\odot}$) that, in the wake of exhausting their Helium-burning core, they are doomed to skip the Asymptotic Giant Branch (AGB) phase; instead they become brighter and then head directly to the white dwarfs (WDs) graveyard.

The vast majority ($\sim 80\%$) of the Milky Way sdBs resides in binary systems; over 50% of which are in close binaries[3]. The unavoidable interactions among the close companions therefore devise a viable mass-loss mechanism capable of stripping the stellar core of its envelope and forming an sdB star. On the other hand, EHBs in GCs display a surprising dearth of binary systems[4–7]. By all means, of the hundreds of EHBs monitored to date, only *one* EHB binary system is known[8]. The shortage of EHB binaries is supported by recent *spectroscopic* monitoring of GCs' red giants inferring a very low ($\lesssim 5\%$) binary frequency[9]. Thereby, and despite numerous scenarios put forward throughout the past ~ 60 years[10,11] (involving an interplay between cluster's age, cluster's central concentration, Helium-enrichment and mixing, CNO abundance, stellar rotation, and extreme mass-loss) EHBs in GCs lack general consensus on a comprehensive formation scenario. In this framework, our findings are likely to provide new impulse in tackling their properties.

Figure 1 summarises the first of our findings: the detection of sinusoidal, single-wave, EHB light modulations having intermediate periodicities ($\sim 2 - 50$ days) and low amplitudes ($\Delta\,U_{Johnson} \sim 0.04 - 0.22\,\mathrm{mag}$). The periodic EHB variability is detected in three GCs, spanning a wide range in metallicity, dynamical history, age, census of multiple-stellar populations, and estimated Helium-enhancement. The above conclusion, coupled with the evident similarity of the variability's periods/amplitudes and shapes (in three GCs) allows us to predict that these EHB variables are ubiquitous among all GCs possessing EHB stars. This prediction is already proven true by independent explorations in other clusters (c.f. Methods). A closer examination of the color-magnitude diagrams in Fig. 2 also shows that the EHB variables embrace a previously identified photometric discontinuity at $\sim 22,500\,\mathrm{K}$ (Momany-jump[12]), and span a temperature range between $\sim 18,000 - 28,000\,\mathrm{K}$, that is, the very temperature range of EHBs. The frequency of EHB variables is inferred by normalising their number to all EHB stars confined within the colour/luminosity range of the variables themselves (c.f. Extended Data Fig. 1). It is remarkably similar: $\sim 13 \pm 4\%$, $\sim 15 \pm 11\%$, and $\sim 12 \pm 5\%$ for NGC2808, NGC6752, and NGC5139, respectively. Thus, whatever is the origin of the EHB variability, it is likely a *universal* phenomenon and it performs similarly in GCs with different properties.

The origin of the uncovered EHB variability is unlikely related to radial pulsation. Indeed, having an extremely thin H-rich envelope, EHBs are relatively too rigid to allow radial pulsation and, if/when present, this occurs at very high frequencies (multi-periodic, milli-mag oscillations). In particular, rapid (pressure-mode) oscillations with periods around $\sim 100 - 200$ seconds have been detected in both field sdBs[13] and GCs' EHBs[14,15], while slow (gravity-mode) oscillations with periods around $\sim 0.7 - 2.0$ hours[16] are solely found in field sdBs. This framework is simply irreconcilable with the much longer $\sim 2 - 50$ day periods reported here. Similarly, the analysis of the EHBs' light curves and complementary spectroscopic radial-velocity monitoring (of few of the detected variables) allow us to definitively discard the binary origin (c.f. Methods and Extended Data Fig. 2 and 3). This is again not surprising, since all previous surveys searching for EHB bina-

ries in GCs have revealed an overall scarcity[4–7]. Having excluded pulsation/binarity, we here propose that the origin of the EHB variability, according to convention[17], is the α^2 Canum Venaticorum (α^2 CVn) phenomenon, afflicting *Magnetic Chemically Peculiar B/A-type* stars (B_P/A_P). B_P stars display superficial over-abundance of certain chemical elements (mostly Silicon and Iron and rare-earth elements) that leads to spatial variations in opacity and subsequent formation of large spots, kept stable (up to several decades) by an underlying magnetic field[18]. Eventually, these spots rotate with the star, hence causing the photometric/spectroscopic variability. A defining characteristic of these magnetic spots is that they should be *dark* in the Far-ultraviolet and *bright* in the optical window[19].

The parallels we draw between the young/massive (few hundred million years, $\sim 1.5-7\,\mathrm{M_\odot}$) B_P stars and the old/low-mass ($\sim 12\,\mathrm{Gyr}$, $\sim 0.48\,\mathrm{M_\odot}$) EHBs might seem bold. However, besides sharing the same superficial temperatures, we also note that B_P and EHBs are characterised by a similar convective-core/radiative-envelope structure, a similar $\sim 10\%$ frequency among their siblings[20], and most importantly, display similar enhancement/depletion patterns of certain chemical elements. The EHB chemical peculiarities are generally attributed to atomic diffusion processes; where heavier elements are pushed upwards while lighter ones are brought downwards. Indeed, EHB stars straddling the M-jump display $\sim 10-20$ times enhancement in Iron[21] (relative to the cluster's average metallicity) and $\sim 5-10$ times depletion in Helium[6] (relative to solar value). Since all EHBs are by definition chemically peculiar[3], the sub-group of EHB variables conceivably[22] display un-even surface chemical distributions, well-suited to exhibit α^2 CVn spot-induced variability. Further confirmation that the EHB variability is consistent with rotating magnetic spots is served when translating the inferred EHB photometric periods into rotation rates. The inferred $\lesssim 10\,\mathrm{km/s}$ are in excellent agreement with spectroscopic studies (c.f. Extended Data Fig. 4).

Figure 3 summarises our modelling (c.f. Supplementary Information) of the light curve of variable vEHB-12 in NGC2808. The favourable location of this EHB variable (at $7.8'$ away from the crowded and noisier cluster centre) has allowed us to exploit *both* the U/R Johnson-filters light curves, simultaneously. In particular, one immediately notes that the $U_{Johnson}$ amplitude is unambiguously *larger* than that in the $R_{Johnson}$ filter. This is in perfect accordance with the requisites of the chemical spots' wavelength dependency[23]. The simultaneous $U_{Johnson}/R_{Johnson}$ light curves modelling converges on the presence of a bright ($\sim 2,500\,\mathrm{K}$ hotter than its surroundings) stellar spot covering as much as $\sim 25\%$ of the EHB surface. Extrapolating from detailed modeling[24,25] of field B_P stars (displaying photometric/spectroscopic/magnetic single-wave modulations, c.f. Supplementary Information) the sizeable spot of vEHB-12 likely reflects the presence of an *off-centre* dipolar magnetic field whose poles are separated only by the spot's diameter ($\sim 60°$). Due to the averaging process over a given hemisphere, similar magnetic field configuration will expectedly deliver, an overall, *weak* field strength measurement.

We take our modelling of the stellar spots a step further and address the question: *why is the α^2 CVn variability detected in only $\sim 13\%$ of the EHBs?* We simulated over 2 milion light curves including a spot with all possible parameters (e.g. size, location, and a given temperature distribution) and then searched among these modelled curves which ones had a variability signal just as strong/high as that seen in the observed EHB variables. Although all simulated light curves

include stellar spots, only $\sim 33\%$ of these match the observed variability signal. Interestingly, assuming a realistic spot temperature distribution, the frequency of detectable EHB variables goes down to $\sim 12\%$ (c.f. Supplementary Information); very close to the empirical frequency inferred for the three examined GCs. This ultimately suggests that the majority of the chemically peculiar EHBs are lurking with small-sized, low-contrast temperature, and unfavourably positioned spots: a true plague of magnetic spots and yet one only recognises the tip of the plagued EHB population.

Detailed modelling[1,26] of hot ($\geq 6,000$ K) horizontal branch stars envisages the presence of surface/sub-surface convective layers (namely the first ionization Hydrogen and the first and second ionization Helium convective zones, HCZ, HeICZ, and HeIICZ). The three layers not only reach up towards the surface of the star but can also, as a function of specific temperatures, merge and/or disappear. Focusing our attention on hot ($\sim 20,000 - 30,000$ K) Hydrogen-rich EHBs, the envelope of these stars is always radiative with a close, sub-surface, HeIICZ layer beneath it. Surprisingly, this detailed EHB envelope structure is *mirrored* in the models of $0.9 - 7\,M_\odot$ young main-sequence (MS) stars[27]. In particular, modelling of the HeIICZ convective layer in main-sequence stars proves it being capable of producing low-level (less than few hundred Gauss) dynamo-generated magnetic fields which, via buoyancy[28], can easily reach the stellar surface and form bright magnetic spots[27]. Of most interest to our proposed EHB/MS parallelism is that the modelling of both EHB[1,26] and MS[27] stars predicts the HeIICZ to approach the (still radiative) stellar surface just around the M-jump temperature, encompassing the EHB variables. Furthermore, the two modelings envisage similar thinness for both the HeIICZ and the radiative layer above it, all taking place in the upper $\sim 1\%$ of the stellar envelope (Supplementary Information). Granted the above similarities, we argue that the HeIICZ's capability of generating magnetic fields in MS stars can be safely extrapolated to EHB stars as well.

Obviously, there are uncertainties in modelling these dynamo-generated magnetic fields (e.g. the geometry of the resulting spots, the strength and lifetimes of the magnetic fields). Moreover, we have just started scratching the surface of the EHB magnetic field properties which, in distant GCs, is hardly detectable with currently available instrumentation. Nonetheless, the stage seems set: there are *four EHB observables* whose onset is temperature ($\sim 22,000$ K) related: (i) the M-jump photometric discontinuity[12]; (ii) the Iron-enhancement discontinuity[21]; (iii) the onset of significant scatter in Helium-abundance[29] and lastly; (iv) the onset of α^2 CVn variability and appearance of magnetic spots/fields. There were already suggestions[21] that the HeIICZ is the triggering mechanism of the first two phenomena and likewise, we here argue it is likely to trigger the third/fourth, too. Our discovery of an *EHB magnetic spot plague*, is however the most revealing: without the HeIICZ-generated magnetic fields the consequent superficial spots cannot be stabilised on time-scales of years, i.e. no magnetic fields, no stable spot-induced EHB variability.

Additional insight into the turbulent nature of the HeIICZ approaching the upper $\sim 1\%$ of the EHB stellar radius may be provided by our second detected variability: low-amplitude ($\Delta\,u_{SDSS} \lesssim 0.1$ mag) luminosity transitions, occurring on time-scales of hundreds of days only in stars hotter than the M-jump (c.f. Fig. 4 and Extended Data Fig. 5). Seven such variables (which we denominate *Padua*) were detected in NGC6752 (the only GC for which we collected a long-term $\sim 6-$year monitoring) and in two cases the luminosity transitions were preceded by mini-bursts. As for the periodic EHB variables, we also preclude binary evolution and stellar pulsation being

the origin of the aperiodic variability. Furthermore, the inferred frequency of the Padua-variables in NGC6752 is $\sim 10\%$, in line with that of the periodic EHB variables.

Padua-1 is an excellent representative of the entire Padua-family as it simultaneously displays a luminosity transition and a mini-burst event. Both are confirmed in the $r-$filter light curve. Since we exclude binary evolution and pulsation, the most immediate framework explaining the Padua-1 mini-burst event is sought in magnetic superflare events. Figure 4 shows the light curve of Padua-1, displaying a full-sampled mini-burst whose: sharp rise/exponential slow decay form, $\Delta u_{SDSS} \sim 0.05$ mag amplitude, ~ 80-day lifetime, and 10^{39-40} erg released energy are consistent with that of a superflare event. Sun-like flares occur when convection in the vicinity of spots[30] distorts the magnetic field which, in turn, pierces the photosphere and connects the corona to the stellar interior. This mechanism releases large quantities of stored magnetic energy. In general, flares last up to few hours. However, evidence exists of superflare events enduring ~ 25 days[31] in F-type stars (releasing $\sim 10^{37}$ erg) and others lasting tens of days[32] in radiative-enveloped B-type stars (releasing $\sim 10^{40}$ erg). The slow EHB rotation velocities (as inferred here from our periodic variables and Kepler-based sdB studies[33]) further provide the necessary grounds for witnessing a long superflare event as in Padua-1. Furthermore, the existence of such energetic/enduring superflares would not be surprising[34] especially if the EHB stars display large-scale spots coverage (e.g. Fig. 3).

To comprehend the energetics involved in the Padua-1 superflare event, one should bear in mind that (even from a Kepler point of view) the spectacular solar flare events would still not qualify[34] our Sun as a flaring star (nor a spotted star for that matter). And yet the detected superflare event in Padua-1 is ~ 10 million times more energetic. Thus, the origin of this rare and possibly devastating event is even harder to model, especially considering its occurrence in radiative-enveloped stars. Nonetheless, we stress the fact that energetic superflares as in Padua-1 may also configure a mass-loss/stellar-wind process, possibly relevant[35] to the low frequency of pressure-mode oscillators among sdBs and maybe to the occurrence of secondary helium-core flashes[36].

In conclusion, the detection of the periodic/aperiodic EHB variabilities in GCs has come as a total surprise. The two types of EHB variability are incorporated within a single theoretical framework and are substantiated by its predictions: *weak* magnetic fields, of only few hundreds of Gauss, *do* trigger discernible observables such as magnetic spots and superflare events. In this regard, we emphasise that the ubiquitous nature of magnetism among EHBs in GCs is very much likely applicable to sdBs in the Galactic field as well. In particular, we argue that the distinctive property of EHBs/sdBs (i.e. dearth *vs* excess in binary frequency) is likely behind the concealing of the magnetic spots/fields signature in sdBs. To test this hypothesis we searched among the small minority ($\sim 20\%$) of apparently single-sdB stars inspecting for spot-induced rotational-modulations and possibly flaring events, and we did find one such trojan-horse: CD-38 222 (c.f. Extended Data Fig. 6). Not only does it display ~ 0.22 days rotational light modulation, but it also exhibits a fortuitous detection of an energetic (10^{35} erg) superflare event. The latter constitutes an ultimate proof of an underlying magnetic field, regardless of its strength and/or detectability. Interestingly, the magnetic field in CD-38 222 was independently investigated[37,38] and inferred to be below ~ 400 Gauss.

The above arguments thereby support a scenario where weak magnetic fields are perfectly capable of triggering discernible observables. These localised/weak magnetic fields are likely responsible for the puzzling chemical anomalies (e.g. horizontal/vertical stratification) and are an excellent candidate for the (long-searched) mass-loss process and rotation-braking, all pertinent to the very formation of EHBs in GCs. This also brings about the possible role of localised/weak magnetic fields (and thereby implied presence of stellar spots) producing other puzzling anomalies in other (convective-enveloped) phases[39]. These are particularly pertinent to old/low-mass stars (similar to those in GCs) for which a confirmed weakened magnetic braking is now established[40]. What is sure is that magnetic fields (although weak and not yet detectable) can no long be considered an exotic feature nor a luxury ingredient reserved only for the closest of stars.

Looking at an even a bigger picture, the implications of the EHBs' universal magnetism extend to *all* B-type radiative-enveloped stars (i.e. young MSs, intermediate-age sdBs, old EHBs and defunct WDs), all showing apparently puzzling rotational photometric variability. In all cases however, the puzzle is/was soon solved by invoking different shades of α^2 CVn variability and weak magnetic fields, despite the radiative-enveloped stars at hand. The full-circle is most evident in the field of young B-type MS stars: passing from "shocking" early reports of rotational variability detections to, nowadays, acceptance-calls[41] openly demanding a *"major revision of stellar physics"* for radiative-enveloped MS stars. Indeed, Kepler/TESS studies now establish[42] that a large ($\sim 40\%$) fraction of B-type stars show photometric variability with periods consistent with the stars' rotation periods (i.e. spot-induced variability). Thus, reluctance to accept the proposed magnetic spots' plague for EHBs is likely to echo the early stages of α^2 CVn detection in B-type MS stars.

Interestingly, hot radiative-enveloped WDs are no exception, and evidence of the presence of dark/bright spot-induced variability is mounting rapidly (c.f. Supplementary Information). The parallelism we draw between the EHB/hot-WD photometric spots' properties is likely to be conceded easily, especially given the imminent EHBs' evolution into WDs. On the other hand however, one is expectedly reluctant when recognising the quite different magnetic properties of EHBs and WDs. In particular, one is understandably intimidated when comparing typically strong magnetic fields detected in WDs (reaching hundreds of milions of Gauss) with the allegedly weak magnetic fields (up to few hundreds Gauss) we propose exist in EHBs. Enough to mention spotted-WDs cases like GD 394 or J1529+2928 (with magnetic fields' estimated upper-limits of $\lesssim 12,000$[43] and $\lesssim 70,000$[44] Gauss, respectively) are yet considered non-magnetic WDs. However, the viability of the suggested EHB/WD magnetic parallelism is soon clear once the EHB-to-WD *shrinkage* in stellar radius is taken into account. Indeed, EHBs/sdBs (with $20,000 \leq T_{eff} \leq 30,000$ K and $\sim 0.45\,R_\odot$) are incapacitated to ascend their programmed AGB phase and instead evolve to slightly brighter luminosities (i.e. lower gravities and larger radii) following which they bypass directly to the WDs ($\sim 0.01\,R_\odot$) stage. This detour typically implies a ~ 45 times shrinkage factor in stellar radius. If so, and assuming that surface magnetic flux is conserved during the collapse, then even a modestly weak ~ 400 Gauss (i.e. the estimated upper limit for the sdB CD-38 222 field) would translate[45] into an impressive $\sim 800,000$ Gauss field acting upon the surface of a WD. Thus, the fact that significant spot-induced variability is reported in apparently non-magnetic WDs strengthens our proposal that weak EHBs' magnetic fields play an important

6

role in *bridging* their magnetic/spots properties with their hot-WDs counterparts. This is further supported by studies[46] concluding that strong WDs' magnetism is not required to produce spots on their surface.

Traditionally, magnetic WDs were sought as the descendents of the magnetic B_P/A_P main-sequence stars, i.e. the WDs' magnetic fields are fossil[47]. However, there is an ongoing debate[48] whether these magnetic fields can be dynamo-generated, in some later evolutionary phase. In this regard, our conclusions supporting the presence of dynamo-generated magnetic fields are tightly connected to the sub-surface HeIICZ and its very-close proximity to the stellar surface. In particular, this HeII convective layer does not date back to the original formation epoch at the main-sequence and is fruit of successive evolution (mergers not excluded). Hence, magnetic EHBs in GCs provide a unique benchmark where to investigate the role of *non-fossil* magnetic fields occurring in currently-single/very-old/low-mass stars, on the verge of becoming WDs.

1. Brown, T. M., et al. The Hubble Space Telescope UV Legacy Survey of Galactic Globular Clusters. VII. Implications from the Nearly Universal Nature of Horizontal Branch Discontinuities. *Astrophys. J.* **822**, 44 (2016).

2. Castellani, M., & Castellani, V. Mass Loss in Globular Cluster Red Giants: an Evolutionary Investigation. *Astrophys. J.* **407**, 649 (1993).

3. Heber, U. Hot Subluminous Stars. *Publ. Astron. Soc. Pac.* **128**, 082001 (2016).

4. Moni Bidin, C., et al. The lack of close binaries among hot horizontal branch stars in NGC 6752. *Astron. Astrophys.* **451**, 499-513 (2006).

5. Moni Bidin, C., Villanova, S., Piotto, G., & Momany, Y. A lack of close binaries among hot horizontal branch stars in globular clusters. II. NGC 2808. *Astron. Astrophys.* **528**, A127 (2011).

6. Moehler, S., et al. The hot horizontal-branch stars in ω Centauri. *Astron. Astrophys.* **526**, A136 (2011).

7. Latour, M., Randall, S. K., Calamida, A., Geier, S., & Moehler, S. SHOTGLAS. I. The ultimate spectroscopic census of extreme horizontal branch stars in ω Centauri. *Astron. Astrophys.* **618**, A15 (2018).

8. Moni Bidin, C., et al. A Hot Horizontal Branch Star with a Close K-type Main-sequence Companion. *Astrophys. J. Lett.* **812**, L31 (2015).

9. Lucatello, S., et al. The incidence of binaries in globular cluster stellar populations. *Astron. Astrophys.* **584**, A52 (2015).

10. Catelan, M. Horizontal branch stars: the interplay between observations and theory, and insights into the formation of the Galaxy. *Publ. Astron. Soc. Pac.* **320**, 261-309 (2009).

11. Gratton, R., et al. What is a globular cluster? An observational perspective. *Astron. Astrophys. Rev.* **27**, 8 (2019).

12. Momany, Y., et al. A New Feature along the Extended Blue Horizontal Branch of NGC 6752. *Astrophys. J. Lett.* **576**, L65-L68 (2002).

13. Kilkenny, D., Koen, C., O'Donoghue, D., & Stobie, R. S. A new class of rapidly pulsating star - I. EC 14026-2647, the class prototype. *Mon. Not. R. Astron. Soc.* **285**, 640-644 (1997).

14. Brown, T. M., Landsman, W. B., Randall, S. K., Sweigart, A. V., & Lanz, T. The Discovery of Pulsating Hot Subdwarfs in NGC 2808. *Astrophys. J. Lett.* **777**, L22 (2013).

15. Randall, S. K., et al. Pulsating hot O subdwarfs in ω Centauri: mapping a unique instability strip on the extreme horizontal branch. *Astron. Astrophys.* **589**, A1 (2016).

16. Green, E. M., et al. Discovery of A New Class of Pulsating Stars: Gravity-Mode Pulsators among Subdwarf B Stars. *Astrophys. J. Lett.* **583**, L31-L34 (2003).

17. Samus', N. N., Kazarovets, E. V., Durlevich, O. V., Kireeva, N. N., & Pastukhova, E. N. General catalogue of variable stars: Version GCVS 5.1. *Astron. Rep.* **61**, 80-88 (2017).

18. Bernhard, K., Hümmerich, S., Otero, S., & Paunzen, E. A search for photometric variability in magnetic chemically peculiar stars using ASAS-3 data. *Astron. Astrophys.* **581**, A138 (2015).

19. Mikulášek, Z., et al. An Overview of the Properties of a Sample of Newly-Identified Magnetic Chemically Peculiar Stars in the Kepler Field. In Kudryavtsev, D.O., et al. (eds.) *Physics of Magnetic Stars*, vol. 518 of *ASP Conference Series*, 117-124 (2019).

20. Bagnulo, S., Landi Degl'Innocenti, M., Landolfi, M., & Mathys, G. A statistical analysis of the magnetic structure of CP stars. *Astron. Astrophys.* **394**, 1023-1037 (2002).

21. Brown, T. M., et al. A Universal Transition in Atmospheric Diffusion for Hot Subdwarfs Near 18,000 K. *Astrophys. J.* **851**, 118 (2017).

22. Paunzen, E., et al. Search for stellar spots in field blue horizontal-branch stars. *Astron. Astrophys.* **622**, A77 (2019).

23. Krtička, J., et al. The nature of light variations in magnetic hot stars. Contributions of the Astronomical Observatory Skalnate Pleso **48**, 170-174 (2018).

24. Shavrina, A. V., et al. Spots structure and stratification of helium and silicon in the atmosphere of He-weak star HD 21699. *Mon. Not. R. Astron. Soc.* **401**, 1882-1888 (2010).

25. Glagolevskij, Y. V., & Chuntonov, G. A. Composite model for the magnetic field of HD 21699. Astrophysics **50**, 362-371 (2007).

26. Cassisi, S., & Salaris, M. *Old Stellar Populations: How to Study the Fossil Record of Galaxy Formation.* (Wiley-VCH, 2013).

27. Cantiello, M., & Braithwaite, J. Envelope Convection, Surface Magnetism, and Spots in A and Late B-type Stars. *Astrophys. J.* **883**, 106 (2019).

8

28. Cantiello, M., & Braithwaite, J. Magnetic spots on hot massive stars. *Astron. Astrophys.* **534**, A140 (2011).

29. Moni Bidin, C., et al. Spectroscopy of horizontal branch stars in ω Centauri⋆. *Astron. Astrophys.* **547**, A109 (2012).

30. Schaefer, B. E. Astrophysics: Startling superflares. *Nat.* **485**, 456-457 (2012).

31. Schaefer, B. E., King, J. R., & Deliyannis, C. P. Superflares on Ordinary Solar-Type Stars. *Astrophys. J.* **529**, 1026-1030 (2000).

32. Schaefer, B. E. Flashes from Normal Stars. *Astrophys. J.* **337**, 927 (1989).

33. Reed, M. D., et al. Analysis of the rich frequency spectrum of KIC 10670103 revealing the most slowly rotating subdwarf B star in the Kepler field. *Mon. Not. R. Astron. Soc.* **440**, 3809-3824 (2014).

34. Balona, L. A. Flare stars across the H-R diagram. *Mon. Not. R. Astron. Soc.* **447**, 2714-2725 (2015).

35. Fontaine, G., Brassard, P., Charpinet, S., & Chayer, P. The need for radiative levitation for understanding the properties of pulsating sdB stars. *Mem. Soc. Astron. It.* **77**, 49 (2006).

36. Miller Bertolami, M. M., Battich, T., Córsico, A. H., Christensen-Dalsgaard, J., & Althaus, L. G. Asteroseismic signatures of the helium core flash. Nature Astronomy **4**, 67-71 (2020).

37. Landstreet, J. D., Bagnulo, S., Fossati, L., Jordan, S., & O'Toole, S. J. The magnetic fields of hot subdwarf stars. *Astron. Astrophys.* **541**, A100 (2012).

38. Bagnulo, S., Fossati, L., Landstreet, J. D., & Izzo, C. The FORS1 catalogue of stellar magnetic field measurements. *Astron. Astrophys.* **583**, A115 (2015).

39. Somers, G., Cao, L., & Pinsonneault, M. H. The SPOTS Models: A Grid of Theoretical Stellar Evolution Tracks and Isochrones for Testing the Effects of Starspots on Structure and Colors. *Astrophys. J.* **891**, 29 (2020).

40. van Saders, J. L., et al. Weakened magnetic braking as the origin of anomalously rapid rotation in old field stars. *Nat.* **529**, 181-184 (2016).

41. Balona, L. A. Evidence for spots on hot stars suggests major revision of stellar physics. *Mon. Not. R. Astron. Soc.* **490**, 2112-2116 (2019).

42. Balona, L. A., et al. Rotational modulation in TESS B stars. *Mon. Not. R. Astron. Soc.* **485**, 3457-3469 (2019).

43. Dupuis, J., Chayer, P., Vennes, S., Christian, D. J., & Kruk, J. W. Adding More Mysteries to the DA White Dwarf GD 394. *Astrophys. J.* **537**, 977-992 (2000).

44. Kilic, M., et al. A Dark Spot on a Massive White Dwarf. *Astrophys. J. Lett.* **814**, L31 (2015).

45. Koester, D., & Chanmugam, G. REVIEW: Physics of white dwarf stars. *Rep. on Prog. in Phys.* **53**, 837-915 (1990).

46. Reding, J. S., Hermes, J. J., & Clemens, J. C. An Exploration of Spotted White Dwarfs from K2. In *Proceedings of the 21st European Workshop on White Dwarfs*, 1-6 (2018).

47. Mestel, L. The magnetic field of a contracting gas cloud. I,Strict flux-freezing. *Mon. Not. R. Astron. Soc.* **133**, 265 (1966).

48. Ferrario, L., Wickramasinghe, D. T., & Kawka, A. Magnetic fields in isolated and interacting white dwarfs. arXiv e-prints arXiv:2001.10147 (2020).

49. Grundahl, F., Catelan, M., Landsman, W. B., Stetson, P. B., & Andersen, M. I. Hot Horizontal-Branch Stars: The Ubiquitous Nature of the "Jump" in Strömgren u, Low Gravities, and the Role of Radiative Levitation of Metals. *Astrophys. J.* **524**, 242-261 (1999).

50. Pietrukowicz, P., et al. Blue large-amplitude pulsators as a new class of variable stars. *Nat. Ast.* **1**, 0166 (2017).

Author Contributions   Y.M. and S.Z. designed the study and coordinated the activity. Y.M., S.Z., M.M., H.M.J.B., D.J., M.G., I.S., L.M., C.M.B., V.D. and H.L. reduced and analysed the data. M.M. and S.Z. developed the spot modelling programme and related simulations. S.C., L.G., and D.J. provided theoretical modelling. G.P., A.P.M., P.B.S., Y.B. and E.M. contributed to the assembly of the photometric catalogs. Y.M. wrote the paper. S.Z., D.J., H.M.J.B., I.S., S.C., L.G. and H.L. contributed to the discussion and presentation of paper. All authors contributed to the discussion of the results and commented on the manuscript.

Competing Interests   The authors declare that they have no competing financial interests.

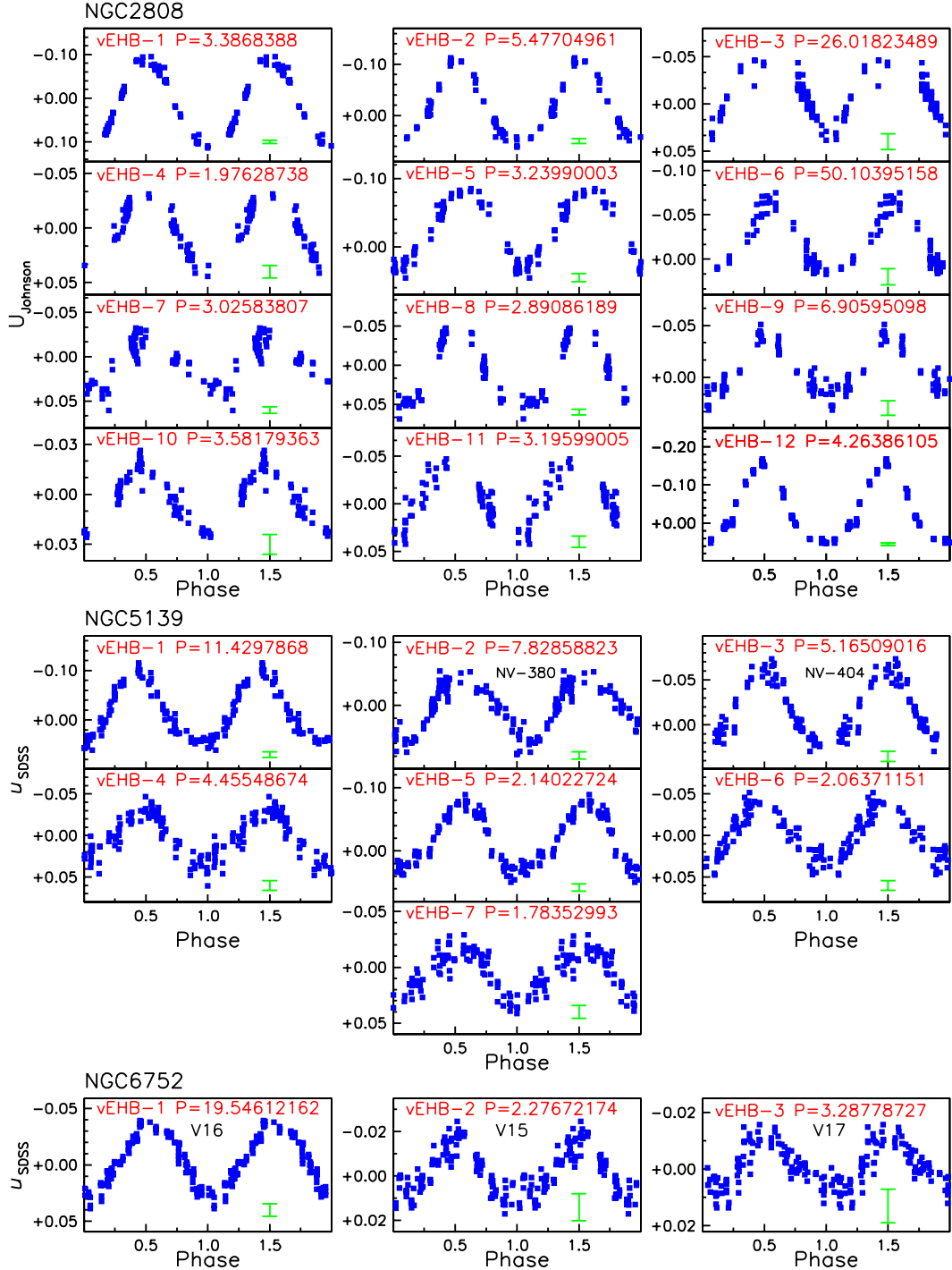**Correspondence**   Yazan Al Momany (email: yazan.almomany@inaf.it)

Figure 1: The phased near-ultraviolet light curves of the EHB variables in three globular clusters. The phased epochs are repeated twice for a better display of the periodicity. We used the $U_{Johnson}$-filter for the NGC2808 data (collected with VIMOS at the UT3 telescope) and the u_{SDSS}-filter for the NGC6752 and NGC5139 data (collected with OmegaCAM at the VST telescope). For each variable we report an assigned-identifier, the photometric period in days, and the typical $1 - \sigma$ photometric uncertainty of the measurements (plotted as an error bar).
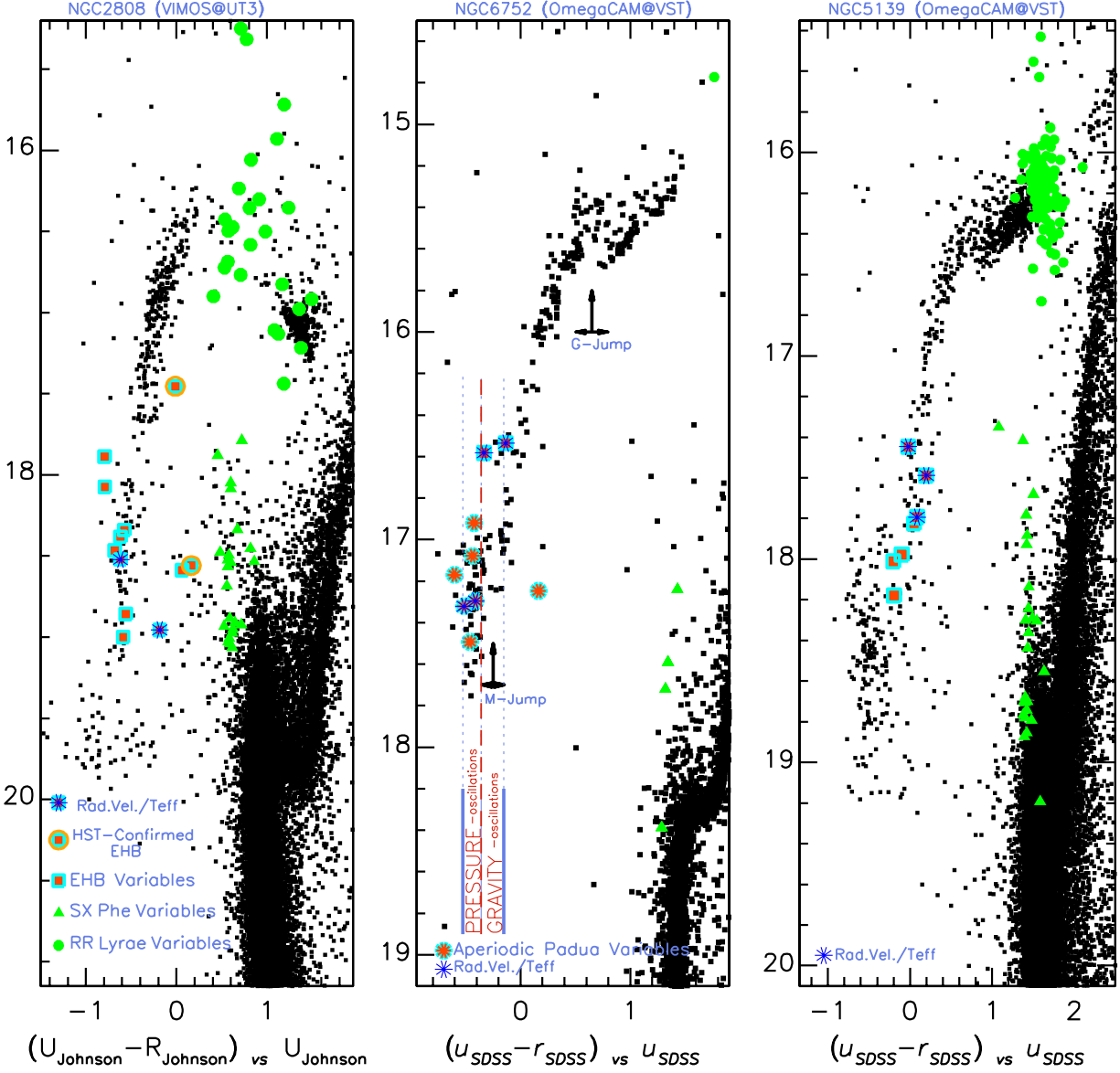
Figure 2: The EHB variables in the near-ultraviolet color-magnitude diagrams. The periodic EHB variables are plotted as filled red squares while the long-term aperiodic Padua variables as filled red asterisks. Stars with spectroscopic data are further highlighted with blue asterisks. Also plotted are the known RR Lyrae and SX Phoenicis pulsators along with the location of the Grundahl-[49] and Momany-[12] jumps (at $\sim 11,500$ and $\sim 22,500\,$K, respectively). The vertical lines in the NGC6752 diagram represent the temperature boundaries[50] of the pressure/gravity mode oscillations.
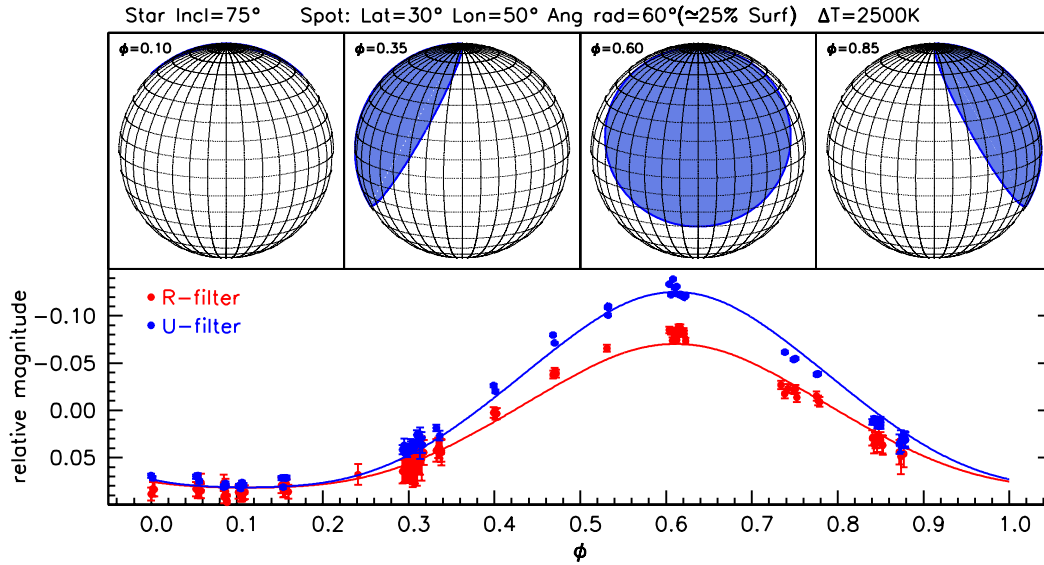
Figure 3: Modelling of the stellar spot in the NGC2808 EHB variable vEHB-12. Lower panel displays the superposition of the $R_{Johnson}$ filter (red circles) and the $U_{Johnson}$ filter (blue circles) light curves, along with the $1 - \sigma$ error bars of each measurements. Solid lines show the corresponding best fitting model for a simulated spotted star, whose modelled *bright* spot's parameters (inclination, longitude/latitude, angular radius, and temperature contrast) are reported. The upper horizontal panels display a snapshot of the modelled spot position (shaded region covering $\sim 25\%$ of the stellar surface) at four key phases during the ~ 4.3-day cycle.

13
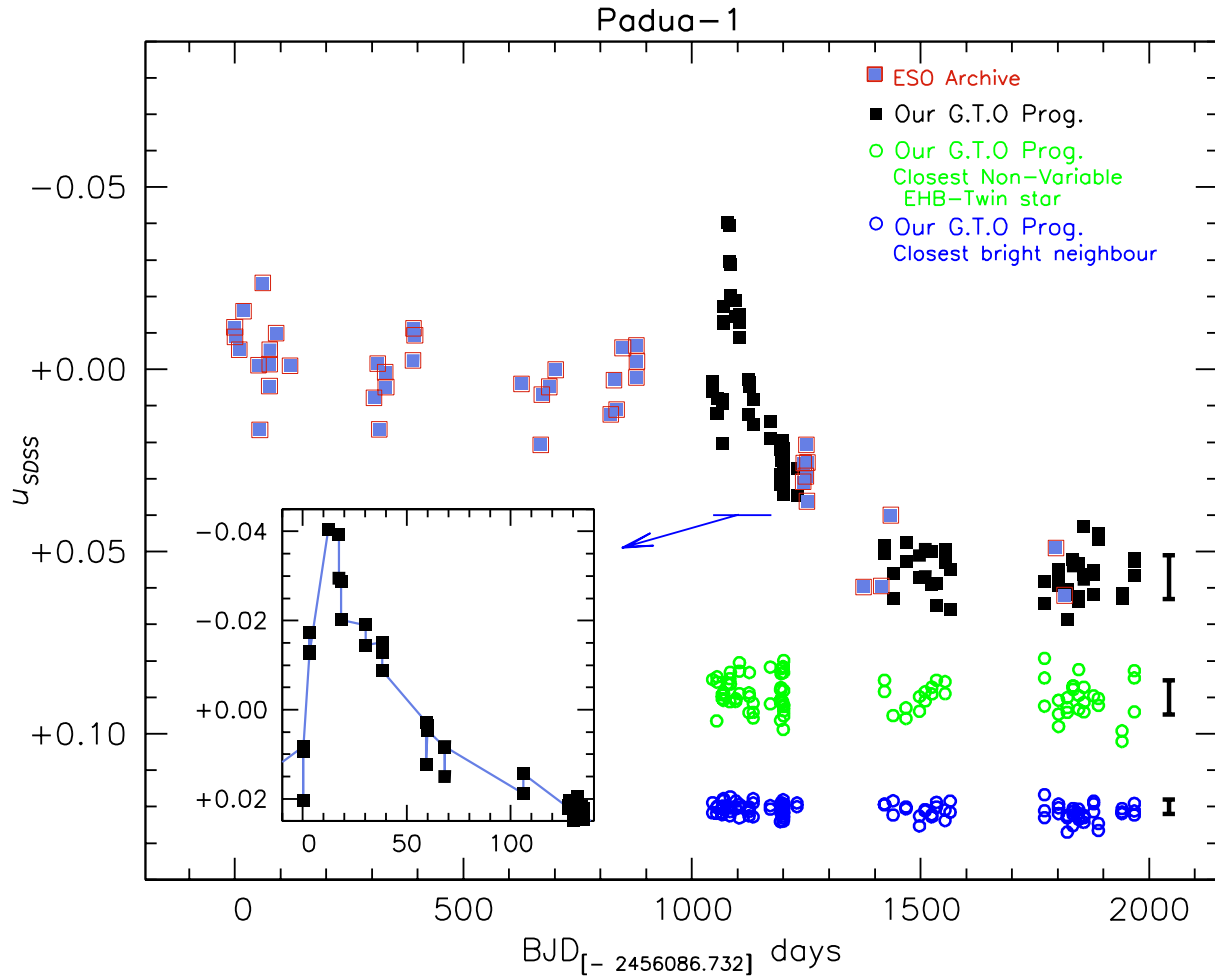
Figure 4: The u_{SDSS} light curve of the EHB Padua-1 showing a complete superflare event. Light blue squares display the six-year monitoring of Padua-1 using archival OmegaCAM@VST data, while black squares display our three-year monitoring using the same instrument/filters/exposure times but collected with better seeing and more frequent sampling. The agreement between the two data-sets is evident. Two comparison stars (green/blue open circles) along with their respective $1 - \sigma$ photometric error bars are also plotted. The constant trends displayed by the comparison stars (at only $\sim 20''$ and $\sim 13''$ from Padua-1) prove that the ~ 0.05 mag fainting and the ~ 80-day superflare event are intrinsic to Padua-1.

14

Methods

Photometric Data Sets

The presented light curves (Fig. 1) and color-magnitude diagrams (Fig. 2) are based on: (i) VIMOS $U_{Johnson}/R_{Johnson}$ photometric data collected at the UT3 telescope of the Very Large Telescope at the ESO Paranal Observatory (Chile); P.I. D. Jones (programme 094.D-0082); (ii) OmegaCAM u_{SDSS}/r_{SDSS} photometric data collected at the VST telescope at Paranal; P.I. Y. Momany (programmes 095.D-0307, 096.D-0021, 097.D-0012 and 099.D-0348) and S. Zaggia (programmes 0100.D-0023 and 0101.D-0171); and (iii) archival OmegaCAM data (programme 60.A-9038). All data presented were collected through the ESO service-mode and are available for download from the ESO archive. VIMOS[1], de-commissioned as of now, was a wide-field imager made of four identical arms, each Quadrant was equipped with a $4\,k \times 2\,k$ CCD having a pixel-size of $0.205''$ and a usable field of view of $7' \times 8'$ per quadrant. We collected 18 epochs of $U_{Johnson}/R_{Johnson}$ exposures of NGC2808 spread between November 20th 2014 and March 12th 2015. Overall, we collected $68 \times 120_{sec}$ images in the $U_{Johnson}$ filter and $91 \times 90_{sec}$ in the $R_{Johnson}$ filter, obtained with excellent ($\sim 0.7''$) seeing conditions as measured in the images. NGC2808 was placed in the center of Quadrant#1, providing a full coverage of the central $\sim 5'$ region. The 3 other quadrants allowed us to sample NGC2808 populations out to $\sim 18'$. A minimum dithering pattern, consisting of only few arcseconds, was employed in order to minimize the introduction of artefacts (e.g. sky concentration, reflection, saturated columns etc). OmegaCAM[2] is the wide-field imager on the $2.6-$m VLT Survey Telescope (VST) telescope. It provides a total un-vignetted field of view of $1° \times 1°$ with a 32-CCD mosaic in a $8^{columns} \times 4^{rows}$ pattern. Each CCD covers a $7.3' \times 14.6'$ field of view, having a pixel size of $0.21''$. For NGC6752 we collected $104 \times 300_{sec}$ and $89 \times 90_{sec}$ u_{SDSS}/r_{SDSS} exposures, respectively. These had an average seeing of $\sim 1.3'$ and $\sim 1.0'$ covering the period between April-2015 and October-2018. For NGC5139 we analysed 89 and 85 u_{SDSS}/r_{SDSS} images collected between April-2015 and May-2017. The two clusters were centered in CCD#84 providing a catalog of $1° \times 1°$. Being part of the calibration plan of the Paranal Observatory, we complement our NGC6752 OmegaCAM data-set with archival images collected with the same instrument/filters/exposure times, between April-2012 and July-2017. The homogeneity of the archival data-set allowed the recovery of $98/90$ images with seeing of $1.4''$ and $1.1''$, in u_{SDSS}/r_{SDSS} respectively. For all OmegaCAM data we made sure that each scientific image was de-biased and flat-fielded with proper images collected within $\sim 2-3$ days from the observations themselves. The entire archival data-set of NGC6752 was reduced independently. Our monitoring of the 3 GCs is still ongoing. We emphasise that NGC6752 is the only GC for which we present u monitoring spanning a period of ~ 6 years, and it is the only one where the long-term variables have been properly identified/investigated.

The photometric reduction of the VIMOS/OmegaCAM dat-sets was based on Point-Spread Function (PSF) photometry that was performed independently on each single image using the PSF-fitting code DAOPHOT II/ALLFRAME[3]. The instrumental photometry was calibrated using linear transformations based on measurements of Peter Stetson complementary photometric standard stars. Our final photometric/astrometric catalogs of the three GCs are photometrically

complete down to ~ 2 magnitudes below the cluster's main sequence turnoff level, and artificial star experiment indicated a $\sim 50\%$ completeness levels at ~ 3 mag below the turnoff levels (c.f. the deepness of diagrams in Fig.2 and error bars in the light curves). This ensured optimal high-precision photometry and completeness of the EHB and the blue hook stars when present.

The light curves were constructed using the differential image subtraction (ISIS2.2) technique[4] which is optimal for the study of crowded fields. Its main advantage is that it does not assume any specific functional shape for the PSF of each image. Instead it models the kernel that convolved the PSF of a reference image (created from the best seeing images) to match the PSF of a target image. The reference image is convolved by the computed kernel and then subtracted from all, single images. We emphasise that the reference image was constructed regardless of the specific epoch of the best-seeing images, hence ensuring a homogeneous treatment of images collected over different observing-seasons. The final photometry on the subtracted images was performed with a, properly modified, DAOPHOT aperture-photometry routine[5]. The aperture photometry radius and inner/outer sky annuli were set for each single image separately, based on the average full-width at half-maximum of the respective image. The absolute time stamp reported in our light curves are the Barycentric Julian Date (BJD[6]) which is referenced to the center of mass of the solar system, and thereby corrects for the Sun's movement due to the gravitational attraction of the planets.

The light curves were examined for variability running the AoV (Analysis of Variance), AOV_HARM (Analysis of Variance using a multi-harmonic model) and LS (Generalised Lomb-Scargle search for periodic sinusoidal signals) algorithms – all found in the VARTOOLS package[7–9]. Thus, for each light curve we searched for periodic signals using the three different algorithms. The average power of the entire sample was derived, and stars with periodic signals power exceeding 3 times the average were folded with their respective period estimates and examined in detail. In particular, the strongest 5-peaks (from each of the 3 algorithm analysis) were examined in order to check for possible aliases. In basically all cases, the peak delivering the least residuals coincided with that being the strongest and the corresponding AOV_HARM period was assumed. All reported variables were visually inspected for neighbour contamination. In particular, the light curves of all neighbours within $\sim 20''$ were thoroughly examined to ascertain that the true variability source is the one we list in Supplementary Table 1. This process was repeated for both the $U_{Johnson}/R_{Johnson}$-filters data independently. We emphasise however that our variability search/analysis (for all 3 GCs) relies primarily on the $U_{Johnson}/u_{SDSS}$-filter light-curves, as these allowed us to suppress the contribution of the (undesired) bright/cool red giant stars and enhance that of the faint/hot stars, the targets of the survey. Indeed, and especially in the central/crowded regions, the $R_{Johnson}/r_{SDSS}$-filter light curves suffered from the high-background and saturation effects which reflected in light curves with lower photometric precision. Among the EHBs presented in Fig. 1 there were few cases of previously identified[10,11] variables (highlighted with their original identifier in Supplementary Table 1 and Supplementary Fig. 7) all of which were *originally* attributed to binary systems. Interestingly, the estimated periods of the common variables shows an excellent agreement (i.e. ~ 2.2 and $\gtrsim 8$ days[11] for vEHB-2/1 in NGC6752, and ~ 5.1 and ~ 7.1 days[10] for vEHB-3/2 in NGC5139). Additional examples of intermediate-period, single-

wave, sinusoidal EHBs variables are found in NGC6656[12] (~ 2.2 days) and NGC6254[13] (~ 0.9 and ~ 4.5 days), in line with the inferred ubiquitous nature, in all GCs hosting EHB stars.

Estimating the NGC2808 EHB variables frequency is summarised in Supplementary Fig. 1. In particular, the two EHB variables (vEHB-7 and vEHB-11 in orange open symbols) were properly identified in higher-resolution Hubble Space Telescope (HST) catalogs[14] and allow us to confidently include them (and the 2 variables they enclose) within the final NGC2808 variable sample. To infer the EHB variable frequency we define the EHB normalising sample as that delimited by the colour/magnitude of the variables themselves. Indeed, as shown in Supplementary Fig. 1, the EHB distribution shows the clear presence of two previously studied[15,16] EHB gaps at $R_{Johnson} \simeq 18.5$ and $\simeq 20.0$, corresponding to $\sim 17,000$ K and $\sim 25,000$ K, respectively. The occurrence/temperature of these gaps is subject to change based on the cluster being examined and/or the filter-set being employed. Hence, the safest selection of the EHB normalising sample is that designed by the EHB variables. Overall, the NGC2808 (periodic) EHB variable frequency is $\sim 13 \pm 4\%$ (12/94), and repeating the same process for NGC6752 and NGC5139 we obtain $\sim 15 \pm 11\%$ (2/13) and $\sim 12 \pm 5\%$ (7/60), respectively. These EHB frequencies may be subject to small fluctuations; due to the inclusion of additional potential variables (see Supplementary Table 1) or the selection of the normalising box colour/luminosity limits. Yet, overall, the EHB variable frequency for the three GCs is very similar, within $\sim 12 - 15\%$. NGC6752 is a particular case where the two identified/confirmed EHB periodic variables span a very limited range in luminosity. Interestingly however, the corresponding normalising EHB population (~ 13 stars) would still deliver an EHB variable frequency of $\sim 15\%$. If we were to include both the periodic/aperiodic EHB variables (i.e. assume that both variability phenomenon represent the stable/eruptive manifestations of magnetic field) the resulting NGC6752 EHB variables frequency is $\sim 11 \pm 4\%$ [(2 + 7)/81].

The temperature range of the EHB variables is inferred from the identification of few of our variables in independent spectroscopic studies. In particular, for NGC2808 vEHB-1 and vEHB-5 we infer $\sim 20,500$ K (see next Section) and $\sim 17,900$ K (holding[5] ID= 42482), respectively. In NGC5139, vEHB-2 (holding[6] ID= 86429) has $28,200$ K, while vEHB-7 and vEHB-4 (holding[7] ID= 5255164 and 5275033) have $23,829$ K and $24,494$ K, respectively. For Padua-1 in NGC6752, we obtain (see Supplementary Information) $29,800$ K. Overall, the EHB variables (of all three GCs) span a temperature range between $\sim 18,000 - 30,000$ K; i.e. closely resembling the very definition of EHBs' temperature range, and never reaching the blue hook temperatures. In this regard, the theoretical ZAHB[17] model (used to constrain the temperatures of the two gaps in Supplementary Fig. 1) further confirms the above inferred temperature range of the EHB variables in NGC2808. Lastly, the case of vEHB-5 in NGC2808 and vEHB-1/2 in NGC6752 caution that the variability may extend to the hotter end of the blue HB; i.e. slightly cooler than the $\sim 20,000$ K nominal EHB cool-boundary.

The lower panels of Supplementary Fig. 1 show the position of all the EHB variables we could identify in available HST catalogs for NGC2808[14], NGC6752[18], and NGC5139[19]. Thanks to their higher-resolution, the HST diagrams show the disappearance of the horizontal bridge con-

necting the EHB to the MS turn-off level (likely caused by photometric blends with undetected faint companions or superposition with foreground/background stars). In this regard, the HST diagrams un-ambiguously show that the EHB variables are anchored to the mean EHB locus; no hints of any particular red-excess. Lastly, we note that if one is to, inappropriately, derive EHB variables frequency using the HST diagrams one would still infer frequencies consistent with those based on our ground-based survey: $\sim 16 \pm 8\%$ and $\sim 10 \pm 6\%$ for NGC2808 and NGC5139, respectively.

EHB Variables Are Not Binary Systems

For a few of our EHB variables we present specific evidence supporting the incompatibility of binary evolution with the detected photometric variability. Variable vEHB-1 in NGC2808 is perhaps the most representative case; since we derived its spectroscopic parameters and monitored its radial velocity over a period matching its photometric period. In particular, a DDT (293.D-5013, P.I. Jones, D.) of 1 hour was granted to obtain optical spectra with the FORS2 spectrograph mounted on the UT1 telescope. Operating through the multi-slit (MXU) mode, on June 23rd 2014 we collected $2 \times 1350_{sec}$ exposures using the $GRIS - 600B$ grism (operating between $3300 - 6210\,\text{Å}$) with a slit width of $1''$ and a resolution of $5.9\,\text{Å}$. The observations were carried out under excellent seeing conditions of $0.8''$, and the scientific frames were de-biased, flat-fielded, and wavelength-calibrated using the FORS2 Reflex-pipeline. The spectra were then extracted with standard IRAF2 routines, corrected for the sky background and flux-calibrated. To derive the effective temperatures, surface gravities, and helium abundances, the observed Balmer and Helium lines were fitted[20] with properly selected stellar model atmospheres. The radial velocity of vEHB-1 confirms it is an NGC2808 member, and we obtain $T_{eff} = 20,500 \pm 2,000\,\text{K}$, $logg = 5.2 \pm 0.3$ and $log(\text{He/H}) = -1.7 \pm 0.3$. The relatively high gravity and low Helium abundance, confirm that the vEHB-1 is a normal EHB star.

As for the radial velocity monitoring, a total of nine spectra were collected (programme 094.D-0363) during three succesive nights between the 11th and 13th December, 2014, using the FLAMES facility mounted at the UT2 telescope in Paranal. The programme, originally[21] aimed at inferring Li and Al abundances of red giants in NGC2808 used the HR15N high-resolution (R= 17000) setup, which simultaneously covers the H_{α} and the Li doublet at $6708\,\text{Å}$. Besides vEHB-1, and for comparison reasons, we monitored a photometrically non-variable EHB, and a known RR Lyrae variable. A radial velocity synthetic template[22] was carefully selected and the standard cross-correlation technique was used to measure the radial velocity of each of the 9 single spectra of each star. The error of the single cross-correlation fit does not reflect the actual error on the radial velocity measurement, and therefore we associate the error on each measurement as that relative to the RMS of the 9 radial velocities, for each star. For the programme stars ($V_{Johnson} \simeq$ 16.5) the RMS of the heliocentric velocity is $\sim 0.8\,\text{km/s}$, and reached ~ 3.5 km/s for our relatively fainter ($V_{Johnson} \simeq 19$) EHB stars, reflecting the natural increase in the RMS as a function of the decreasing S/N. The upper panel of Supplementary Fig. 2 proves the succesful detection of velocity variations in the comparison RR Lyrae star and shows an excellent agreement between the newly derived spectroscopic period and its photometric period of $\sim 0.589\,\text{days}$. The lower

panel however, shows that the RMS of the measured radial velocities of vEHB-1 (~ 2.5 km/s) is comparable to the typical ~ 3.5 km/s errors, estimated for single measurements.

Similarly, Supplementary Fig. 3 presents similar radial velocity monitoring collected for the EHB variables in NGC6752. Relative to those in NGC2808, the NGC6752 EHB variables are ~ 2.5 magnitudes brighter ($V_{Johnson} \sim 16.5$). The spectroscopic data consist of 6 FLAMES archival 2775_{sec} spectra (programme 099.D-0527) collected between June, 22nd and June 30th, 2017. The NGC6752 EHB photometric variables and the original targets of the programme (main sequence stars) basically share the same luminosity, hence, the S/N of both types of stars are similar. The spectra were collected through the *blue* LR02 setup ($R \sim 6000$) operating between $3960 - 4570$ Å. This spectral coverage thus included the H_γ and H_δ and three Helium lines. We therefore employed a minimisation method, comparing the target spectrum with a library of synthetic spectra[22]. Once again we use the RMS distribution as a tracer of error associated to each of the 6 measurements, which for our EHB variables is around ~ 3 km/s. The comparison SX Phoenicis photometric variable shows clear signs of velocity modulations whereas the vEHB-1/2 variables (and the potential EHB candidate vEHB-4/V17), again, display velocity RMS comparable to the error estimated for single measurements.

Lastly, no significant radial velocity variations were independently inferred for two EHB variables included in published monitoring surveys: (i) vEHB-5 in NGC2808[5]; and (ii) vEHB-2 in NGC5139[6]. Thus, it is rather unlikely that the EHB variability is related to close-binary evolution. One may argue that within the achieved ($\lesssim 4$ km/s) radial velocity precision there still may hide the imprint of low-mass stellar/sub-stellar companions that introduce the EHB variability. Indeed, the general shape of the EHB light curves seem fairly typical for an irradiated binary, i.e. a binary system where a hot star irradiates the near face of a cool companion (e.g., the case of HW Vir binaries). Nonetheless, one is readily reminded that the ~ 3.3-day period of vEHB-1@NGC2808 is ~ 4 times longer than the longest (~ 0.75 days[3]) period member of this class.

Examined in further detail, in an irradiated binary, it is the differing projection of this heated face that produces the sinusoidal shape of the light curve. The amplitude of an observed irradiation effect is heavily dependent on multiple factors including the observed wavelength, temperature difference between the two components, orbital separation, and the stellar radii[23]. Our analysis of the spectra of vEHB-1@NGC2808 indicates that its temperature is of the order $\sim 20,500$ K. It is safe to conclude that it should be the irradiating star in this hypothetical irradiated binary. In order to test this hypothesis, an array of models were produced using the binary modelling software PHOEBE2[24] each of which comprised a primary consistent with the observed parameters of vEHB-1@NGC2808 in a ~ 3.3-day orbit with a MS companion of varying spectral type (whose parameters have been adopted from a set of zero age main sequence stellar models[25]). It is clear from the observed light curves that no eclipses are present, so orbital inclinations were limited to be less than $75°$ and any models which presented eclipses were discarded. In all cases, the amplitude of the simulated irradiation effect was much lower than that observed for vEHB-1@NGC2808: for example an approximate K0 companion at an inclination of $75°$ displays a semi-amplitude of approximately ~ 0.02 mag in the $R-$band. This raises the possibility that rather than being

a main sequence star, the companion could be a red giant. However, if the companion would be an RGB star, it would almost certainly be more luminous than vEHB-1, a possibility that is ruled out by the robust identification of the star in the WFC3@HST catalog and its position in the ground/space-based diagrams. Furthermore, in all of the aforementioned models, the amplitude of the effect was, as expected in the irradiation scenario, greater in the $R-$band than in the $U-$band[26], at odds with the observed $U_{Johnson}/R_{Johnson}$ light curves amplitude (see also Fig. 3). This evidence allows us to discard the possibility that vEHB-1 is an irradiated binary (irrespective of whether the secondary is a low-mass MS-star or even a planet). Lastly, concerning the possible detection of planets around EHBs (as is now frequently observed around white dwarfs) we note that several ground/space based surveys aimed at determining the occurrence rate of planets in GCs have yielded null detections[27–29]. This dearth of planets has been attributed to two distinctive properties of GCs; their low-metallicity and the high stellar densities.

An alternative binary interpretation for the light curve is that the variability actually arises from a so-called ellipsoidal modulation, whereby one component is so close to filling its Roche-lobe that the varying projection of its tidally distorted shape reflects an episodic modulation in the light curve. In this scenario, the Roche-lobe-filling star must be the EHB star - otherwise the modulated companion would be dominant in the observed spectroscopy - and the orbital period must be twice the apparent photometric period (as ellipsoidal modulation produces two minima per period[30]). This would offer a natural explanation for the almost similar $R_{Johnson}$ and $U_{Johnson}$ amplitudes as the tidal distortion does not alter with the adopted photometric passband. However, this interpretation is clearly unfeasible given that the mass of the companion required to introduce significant tidal distortion in the EHB for a period of ~ 6.8 days is prohibitively large, while its radius would have to be exceptionally small in order to not overflow its own Roche lobe. Therefore, we can also discard ellipsoidal modulation as a potential source of the EHB photometric variability.

Thus, analysis of the period and $U_{Johnson}/R_{Johnson}$ amplitude of vEHB-1@NGC2808 seems to preclude the viability of either the irradiated/ellipsoidal binary scenario being responsible for the observed luminosity variations. This analysis, coupled with the lack of any significant radial velocity variations, allows us to firmly preclude binarity. Obviously, eventual presence of companions in wide-orbits (e.g. orbital period of ~ 1000 days[31]) cannot be excluded at the moment. However, besides the fact that such wide-binaries are easily destroyed in the dense GC environment, their eventual presence is unlikely to be the cause of the strong and ~ 3-day short-period modulations detected here.

KSint: http://eduscisoft.com/KSINT/index.php
EXOFAST: http://astroutils.astronomy.ohio-state.edu/exofast/limbdark.shtml
ISIS: http://www2.iap.fr/users/alard/package.html
VARTOOL: https://www.astro.princeton.edu/~jhartman/vartools.html
SM: https://www.astro.princeton.edu/~rhl/sm/
ALAMBIC: https://esosoft.univie.ac.at/software/esomvm/
DAOPHOT: http://www.star.bris.ac.uk/~mbt/daophot/

1. Le Fèvre, O., et al. Commissioning and performances of the VLT-VIMOS instrument. *Proc. of SPIE* **4841**, 1670-1681 (2003).

2. Kuijken, K. OmegaCAM: ESO's Newest Imager. *The Messenger* **146**, 8-11 (2011).

3. Stetson, P. B. DAOPHOT: A Computer Program for Crowded-Field Stellar Photometry. *Publ. Astron. Soc. Pac.* **99**, 191 (1987).

4. Alard, C., & Lupton, R. H. A Method for Optimal Image Subtraction. *Astrophys. J.* **503**, 325-331 (1998).

5. Montalto, M., et al. A new search for planet transits in NGC 6791. *Astron. Astrophys.* **470**, 1137-1156 (2007).

6. Eastman, J., Siverd, R., & Gaudi, B. S. Achieving Better Than 1 Minute Accuracy in the Heliocentric and Barycentric Julian Dates. *Publ. Astron. Soc. Pac.* **122**, 935 (2010).

7. Hartman, J. D., & Bakos, G. Á. VARTOOLS: A program for analyzing astronomical time-series data. *Astronomy and Computing* **17**, 1-72 (2016).

8. Schwarzenberg-Czerny, A. Fast and Statistically Optimal Period Search in Uneven Sampled Observations. *Astrophys. J. Lett.* **460**, L107 (1996).

9. Schwarzenberg-Czerny, A., & Beaulieu, J.-P. Efficient analysis in planet transit surveys. *Mon. Not. R. Astron. Soc.* **365**, 165-170 (2006).

10. Kaluzny, J., et al. Cluster AgeS ExperimentCatalog of variable stars in the globular cluster ω Centauri. *Astron. Astrophys.* **424**, 1101-1110 (2004).

11. Kaluzny, J., & Thompson, I. B. Variable Stars in the Globular Cluster NGC 6752. *Acta Astron.* **59**, 273-289 (2009).

12. Rozyczka, M., et al. The Cluster AgeS Experiment (CASE). Variable Stars in the Field of the Globular Cluster M22. *Acta Astron.* **67**, 203-224 (2017).

13. Rozyczka, M., et al. The Cluster AgeS Experiment (CASE). Variable stars in the field of the globular cluster M10. arXiv e-prints arXiv:2001.01529 (2020).

14. Milone, A. P., et al. The Hubble Space Telescope UV Legacy Survey of Galactic Globular Clusters. III. A Quintuple Stellar Population in NGC 2808. *Astrophys. J.* **808**, 51 (2015).

15. Ferraro, F. R., Paltrinieri, B., Fusi Pecci, F., Rood, R. T., & Dorman, B. Multimodal Distributions along the Horizontal Branch. *Astrophys. J.* **500**, 311-319 (1998).

16. Bedin, L. R., et al. The anomalous Galactic globular cluster NGC 2808. Mosaic wide-field multi-band photometry. *Astron. Astrophys.* **363**, 159-173 (2000).

17. Pietrinferni, A., Cassisi, S., Salaris, M., & Hidalgo, S. The BaSTI Stellar Evolution Database: models for extremely metal-poor and super-metal-rich stellar populations. *Astron. Astrophys.* **558**, A46 (2013).

18. Nardiello, D., et al. The Hubble Space Telescope UV Legacy Survey of Galactic Globular Clusters - XVII. Public Catalogue Release. *Mon. Not. R. Astron. Soc.* **481**, 3382-3393 (2018).

19. Cool, A. M., et al. HST/ACS Imaging of Omega Centauri: Optical Counterparts of Chandra X-Ray Sources. *Astrophys. J.* **763**, 126 (2013).

20. Moni Bidin, C., Moehler, S., Piotto, G., Momany, Y., & Recio-Blanco, A. Spectroscopy of horizontal branch stars in NGC 6752. Anomalous results on atmospheric parameters and masses. *Astron. Astrophys.* **474**, 505-514 (2007).

21. D'Orazi, V., et al. Lithium abundances in globular cluster giants: NGC 1904, NGC 2808, and NGC 362. *Mon. Not. R. Astron. Soc.* **449**, 4038-4047 (2015).

22. Coelho, P. R. T. A new library of theoretical stellar spectra with scaled-solar and α-enhanced mixtures. *Mon. Not. R. Astron. Soc.* **440**, 1027-1043 (2014).

23. Jones, D., & Boffin, H. M. J. Binary stars as the key to understanding planetary nebulae. *Nat. Ast.* **1**, 0117 (2017).

24. Prša, A., et al. Physics Of Eclipsing Binaries. II. Toward the Increased Model Fidelity. *Astrophys. J. Suppl.* **227**, 29 (2016).

25. Bertelli, G., Girardi, L., Marigo, P., & Nasi, E. Scaled solar tracks and isochrones in a large region of the Z-Y plane. I. From the ZAMS to the TP-AGB end for 0.15-2.5 M$_\odot$ stars. *Astron. Astrophys.* **484**, 815-830 (2008).

26. Hillwig, T. C., et al. Observational Confirmation of a Link Between Common Envelope Binary Interaction and Planetary Nebula Shaping. *Astrophys. J.* **832**, 125 (2016).

27. Gilliland, R. L., et al. A Lack of Planets in 47 Tucanae from a Hubble Space Telescope Search. *Astrophys. J. Lett.* **545**, L47-L51 (2000).

28. Nascimbeni, V., Bedin, L. R., Piotto, G., De Marchi, F., & Rich, R. M. An HST search for planets in the lower main sequence of the globular cluster NGC 6397. *Astron. Astrophys.* **541**, A144 (2012).

22

29. Wallace, J. J., Hartman, J. D., & Bakos, G. Á. A Search for Transiting Planets in the Globular Cluster M4 with K2: Candidates and Occurrence Limits. *Astronomical. J.* **159**, 106 (2020).

30. Santander-García, M., et al. The double-degenerate, super-Chandrasekhar nucleus of the planetary nebula Henize 2-428. *Nat.* **519**, 63-65 (2015).

31. Vos, J., Németh, P., Vučković, M., Østensen, R., & Parsons, S. Composite hot subdwarf binaries - I. The spectroscopically confirmed sdB sample. *Mon. Not. R. Astron. Soc.* **473**, 693-709 (2018).

Supplementary Information for

A Plague of Magnetic Spots Among the Hot Stars of Globular Clusters

Y. Momany[1], S. Zaggia[1], M. Montalto[2], D. Jones[3,4], H.M.J. Boffin[5], S. Cassisi[6,7], C. Moni Bidin[8], M. Gullieuszik[1], I. Saviane[9], L. Monaco[10], E. Mason[11], L. Girardi[1], V. D'Orazi[1], G. Piotto[2], A.P. Milone[2], H. Lala[2], P.B. Stetson[12] & Y. Beletsky[13]

[1] *INAF - Osservatorio Astronomico di Padova, Vic. dell'Osservatorio 5, 35122 Padova, Italy*
[2] *Dipartimento di Fisica e Astronomia, Univ. di Padova, V. dell'Osservatorio 3, 35122 Padova, Italy*
[3] *Instituto de Astrofisica de Canarias, E-38205 La Laguna, Tenerife, Spain*
[4] *Departamento de Astrofisica, Universidad de La Laguna, E-38206 La Laguna, Tenerife, Spain*
[5] *European Southern Observatory, Karl Schwarzschild Strasse 2, D-85748 Garching, Germany*
[6] *INAF - Osservatorio Astronomico d'Abruzzo, Via M. Maggini, I-64100 Teramo, Italy*
[7] *INFN - Sezione di Pisa, Largo Pontecorvo 3, 56127 Pisa, Italy*
[8] *Instituto de Astronomía, Universidad Católica del Norte, Av. Angamos 0610, Antofagasta, Chile*
[9] *European Southern Observatory, Alonso de Cordova 3107, Santiago, Chile*
[10] *Departamento de Ciencias Fisicas, Universidad Andres Bello, Fernandez Concha 700, Las Condes, Santiago, Chile*
[11] *INAF - Osservatorio Astronomico di Trieste, Via G.B. Tiepolo, 11, I-34143, Trieste, Italy*
[12] *Herzberg Astronomy and Astrophysics, National Research Council, 5071 West Saanich Road, Victoria, BC V9E 2E7, Canada*
[13] *Las Campanas Observatory, Carnegie Institution of Washington, Colina el Pino, Casilla 601, La Serena, Chile*

Supplementary Discussion

The Stability of Magnetic Spots: The parallelism we draw between the α^2 CVn variability in magnetic B_P stars and our EHB variables implies that the EHB variability should be stable on time-scales of years. Supplementary Fig. 4 displays the six phased one-year light curves of vEHB-1/V16 in NGC6752 ($P \sim 19.5$ days) along with the integrated six-year curve and its corresponding best fitting model. Although the measurements originate from two different OmegaCAM data-sets, overall, there are no appreciable phase and amplitude differences among the six one-year light curves with respect to the integrated model. One therefore concludes that the observed EHB variability - attributed to magnetic spots - is stable on a timescale of years as is expected if belonging to the α^2 CVn family.

The confirmed long-term stability of magnetic spots allows us to probe an important stellar property: rotation. A rotating stellar spot is an excellent probe of the *stellar* rotation, to the degree of being considered *superior*[1] to the spectroscopic *v sin i* measurements (which include assumptions on the rotation axis inclination). For example, a modelling of the $T_{eff} \sim 20,500$ K vEHB-1 variable in NGC2808 implies a radius of $\sim 0.45\,R_\odot$, which combined with a photometric period of ~ 3.3 days, translates into a stellar rotation velocity of ~ 6.1 km/s. This is in *perfect* agreement with conclusions of EHB *v sin i* studies (specifically in NGC2808[2]) being $\lesssim 10$ km/s. Repeating the same exercise, the $\sim 2 - 50$ days period distribution translates to a rotational velocity range between $\sim 0.4 - 10.0$ km/s. The ~ 0.4 km/s lower limit, lends support to earlier suggestions[2] that a small NGC2808 EHB population may display extremely low ($\lesssim 2$ km/s) rotational velocities. This overall consistency lends further support to the α^2 CVn framework in explaining the EHB variability.

Magnetism in Radiative Envelopes: We emphasise that whereas the envisaged dynamo-generated magnetic fields actually *reach* the stellar surface[3], the trigger itself (i.e. HeIICZ) *remains*[4–6] *a sub-surface* layer (beneath a very-thin radiative layer) for the *entire* temperature range of our EHB variables. Indeed, atomic diffusion (in and around the EHB variables) is far from being suppressed by HeIICZ surface convection and, if anything, it gets weirder. In particular, we recall that the measured[7] surface Helium-abundances shows a smooth, increasing, trend between $\sim 15,000$ K ($Y \sim 0.008$) and $\sim 20,000$ K ($Y \sim 0.05$). However, for EHBs hotter than the M-jump, this trend is suddenly broken and replaced by a significant dispersion in surface Helium-abundances: varying anywhere between $0.001 \lesssim Y \lesssim 0.1$ on a star-to-star basis. Thus, the empirical Helium-abundance framework is still in perfect agreement with the EHBs' radiative envelopes showing diffusion effects and a general Helium-depletion. In this regard, one must bear in mind that an average EHB measured Helium-abundance of $Y \sim 0.05$ (still sign of "Helium-depletion") is still one order of magnitude *larger* than that theorised/expected assuming an equilibrium between the competing gravitational settling and radiative levitation processes. Weak stellar winds rendering less-efficient the impact of gravitational settling on Helium-depletion is one possible scenario proposed to solve the above mentioned Helium-depletion discrepancy[8].

Overall, the onset of significant Helium-abundance dispersion (in correspondence of the M-jump temperature) and the measured Helium-abundances being anyways larger than expected are both suggestive of the onset of an atmospheric process. The alternating appearance/disappearance of magnetic spots thus provides a viable channel through which randomised enhancement/depletion in Helium are generated. At the same time, the thereby implied presence of *weak* magnetic fields will necessarily trigger some low level of stellar winds that may retard the effects of gravitational settling and, relatively, "increase" the Helium-abundance. Alleged stellar winds in sdBs/EHBs bring about an-

other potential parallelism with young B-type MS stars where chemical peculiarities (such as the [3]He-isotope anomaly and occurrence of Helium rich/poor stars) were linked[9] to similarly *weak* stellar winds and *low* mass-loss rates.

Modelling of a Stellar Spot: First, the surface of vEHB-12 in NGC2808 was approximated by a blackbody model with a temperature of $\sim 20,500\,\mathrm{K}$ as derived from the average $(U_{Johnson} - V_{Johnson})$ color. Second, the emission originating from the spot was simulated using a grid of blackbody temperatures varying between $16,500$ and $28,500\,\mathrm{K}$, and *contrast ratios* between the star/spot emission were derived using the $U_{Johnson}/R_{Johnson}$ filter transmission curves. The limb darkening quadratic coefficients in the $U_{Johnson}/R_{Johnson}$ filters were obtained from the EXOFAST[10] routine. The light curve simulations were generated using the KSɪɴᴛ software[11] which integrates the total emission from the spotted star, incorporating the full-grid of the spot's properties (longitude/latitude/dimension and temperature). These simulations were later repeated varying the star's inclination angle with respect to the line of sight. We then, simultaneously, fit the *observed* $U_{Johnson}/R_{Johnson}$ light curves to the full-grid of *simulated* models, searching for solutions that minimise the χ^2 residuals and lower the spot's temperature contrast. Figure 3 (in the Main text) shows the best simultaneous modelling of the spot in vEHB-12 and converges on the presence of a single, giant and bright ($\sim 2,500\,\mathrm{K}$ hotter than its surroundings) stellar spot covering as much as $\sim 25\%$ of the EHB surface. The high temperature-contrast estimated for the spot in vEHB-12 is however in line with the trend of increasing spot/surrounding-photosphere temperature-contrast with increasing stellar effective temperature[12]. In particular, whereas typical spots' temperature-contrasts for M-type stars are estimated around $\sim 350\,\mathrm{K}$, these reach $\sim 1,400\,\mathrm{K}$ for G-type stars, and are expectedly higher for B-type stars.

One might be puzzled as to how *all* of our EHB light curves are characterised by single-wave photometric modulation. In this regard, we draw parallels to applications of the oblique rotator model[13] (*i.e. a dipole magnetic field whose axis is tilted with respect to the rotation axis*) that successfully reproduced[14] the *simultaneous* occurrence of single-wave photometric/spectroscopic/magnetic modulation in a B_P Helium-poor HD 21699 star. In principle, it envisages one large Helium-spot around one of the magnetic poles while a Silicon-spot is at the opposite pole. However, and in order to avoid the occurrence of *double-wave* modulation, the dipolar magnetic field necessarily needed to be *off-centre*[15]; i.e. displaced from the star's centre by a given distance (smaller than the stellar radius). The resultant configuration is one in which the two magnetic poles are now *closer* to each other on the stellar surface (unlike that of a *centrally* dipole field where the poles are separated by $180°$). The two, *nearby*, poles will then confine *a* single/large spot of, say, Helium-enhanced region, while the Helium-depleted/Silicon-enhanced spot lies on the opposite hemisphere[16].

Although maximum Helium-abundance is expected at the two closely-positioned magnetic poles, these two poles are not actually "resolved". As a result, the Helium-enhanced spot coincides with the poles' *average/intermediate* position. Thus, owing to this *averaging* process over a given hemisphere, *a single* Helium-spot is observed and the overall Helium-abundance is maintained *low*, as for HD 21699. Along these lines, we note that the observed *uvby* single-wave light curves (of a magnetic B_P Helium-rich HD 37776 star[17]) were successfully reproduced, both in shape and amplitude, by introducing ad-hoc enhancement/depletion in surface Helium/Silicon abundances in the observed spectra (aka magnetic spots), later used to recover the correspondent (variable) flux in the *uvby* filters. A similar analysis, assuming other elements of relevance (e.g. Iron/Helium for our EHB variables) is desirable, but requires (currently unavailable) surface chemical composition maps. Lastly, we note

that similarly configured *off-centre* dipolar magnetic fields generally provided[18] a better reproduction of spectroscopic observations for magnetic white dwarfs.

Thus, the modelled giant *bright* spot occupying $\sim 25\%$ of the stellar surface of vEHB-12 (c.f. Fig. 3 of the Main text) would represent a $\sim 3,000$ times scaled-up version of a typical solar dark spot, where the *vertical* magnetic field lines are seen ascending/descending from the poles of the magnetic spot in one hemisphere, while on the opposite hemisphere, the magnetic field lines are predominantly *tangential/horizontal*. This vEHB-12 giant spot configuration, especially that regarding its putative magnetic poles being separated by $\sim 60°$, also implies that the imprint of the ascending/descending vertical/longitudinal magnetic lines will be *washed out* when measuring the *global* longitudinal magnetic field in the visible hemisphere; i.e. reflecting the presence of overall *weak* magnetic fields.

Why Not All ? Puzzled by the very similar EHB variable frequency in the 3 GCs we took our simulations a step further and evaluated the *impact* of the stellar spot properties on the recovered EHB variables fraction. In this regard, we first simulated a full-set of models that take into account all possible parameters characterising the stellar spot (i.e. its latitude, dimension, and temperature contrast). Each of these models were then re-generated with different photometric periods and viewing angles of the star. In particular, we employ the same KSINT software used to generate $U_{Johnson}$ filter light curves with stellar spots having: (i) temperature between $17,000 - 24,000$ K, ranging in steps of 250 K; (ii) latitudes between $-90° \div 90°$, ranging in steps of $10°$; (iii) angular spot dimensions between $10° \div 90°$, ranging in steps of $10°$; (iv) fifty photometric periods randomly selected between $2.0 - 10.0$ days; and (v) stellar inclination angles between $0° \div 90°$ ranging in steps of $10°$. These light curves were simulated using our NGC2808 VIMOS time-sampling and typical $U_{Johnson}$ filter photometric errors generated randomly for each simulated light curve, and then re-run through the AoV_HARM algorithm to derive the False-Alarm-Probability and the photometric $U_{Johnson}$ amplitude, as done for the *observed* light curves. Overall, the library of simulated models included a total of $2,167,854$ light curves.

The lower limits of the $U_{Johnson}$ amplitude and the AoV_HARM false-alarm-probability as determined for the NGC2808 *observed* light curves are $\Delta U_{Johnson} \sim 0.06$ mag and $\sim 10^{-11}$, respectively. The *simulated* light curves that had a *larger* $U_{Johnson}$ amplitude and *lower* false-alarm-probability (than these limits) were selected and their frequency was found to be $\sim 33\%$. This is already a very significant result: assuming a flat distribution - of all possible geometric properties/projections of the stellar spots - would already imply that two-thirds of all simulated models *do not* match the observed (amplitude/false-alarm-probability) properties. In particular, the recovery of $\sim 33\%$ should be considered as an *upper limit* because the library of modelled light curves does not take into account the *real* (and unknown) distribution of the spot's physical properties. This is to say that, for the time being, we do not know of any *preferential* dimension/latitude distributions (e.g. preferential latitude location of spots and spot cycles as in our Sun) of the stellar spots. Thereby all these values are considered equally possible, and their impact is hardly accountable for. On the other hand, the distribution of the spot's temperature contrast (ΔT) is *unlikely* to be a random function, because quite simply the observed EHB variables showing the highest U-amplitudes are a minority. We therefore make the reasonable assumption that the underlying distribution of the spot's ΔT is not-flat and (as compared to the star's average temperature fixed at $20,500$ K in all simulations) follows a Gaussian function with a standard deviation σ that is anywhere between $500 \div 2,500$ K. Assuming the aforementioned Gaussian function and realising $1,000$ experiments (each including 94 light curves

as our reference EHB sample) for a given σ we derive the frequency of the simulated light curves satisfying our measurement constraints. We find that the best re-production of the properties of our EHB variables is obtained with a $\sigma = 1,000\,\mathrm{K}$ Gaussian distribution that includes (at a $\sigma \sim 2.2$ level) the $\Delta T \sim 2,500\,\mathrm{K}$ estimated for vEHB-12, which is our largest amplitude variable. Granted the above, we infer that the frequency of the spotted/simulated light curves that satisfies our observed constraints could go down to $\sim 12.3 \pm 3.7\%$. This is surprisingly similar to the observed frequency. Many unknowns can alter this estimate (e.g. the presence of more than one spot, the eventual geometrical distribution of these multiple spots, etc). However, any further sophistication of our first-order simulations is likely to introduce uncertainties of its own. The above simulations clearly indicate that the spots' specific properties heavily affect the detectable variability fraction. Overall, the observed EHB variable frequency $\sim 12 - 15\%$ in the 3 GCs is yet compatible with the spot phenomenon being a wide-spread feature, lurking at some level, among these certainly chemically peculiar EHB stars.

Lastly, we emphasise that the above simulations (and the important implications they deliver) were made possible thanks only to the availability of a, sizeable, homogeneous EHB sample (sharing basically the same distance, age, and metallicity) monitored by a single photometric survey (with known photometric precision, depth and completeness). Similar procedures are hardly applicable to field sdBs *sparsely* distributed in the Milky Way field subject to intrinsic uncertainties in distance, reddening, age, and original MS chemical composition.

The Padua EHB variables: Supplementary Fig. 5 displays the light curves of the remaining six, aperiodic, EHB (*Padua*) variables. NGC6752 is the only cluster for which we could integrate our 3-year data with existing 6-year archival data. The case of *Padua-7* is quite instructive: once a luminosity transition has taken place (in about $400-500\,\mathrm{days}$) the EHB star displayed an overall consistent luminosity for the following ~ 4 years; belying a "constant" star profile. Thus, *only* long-term, high-precision, regular monitoring can reveal the presence of *Paduas*, and we suspect more of them exist not just in NGC6752 but in other GCs as well. Gaia proper-motion determinations of the *Padua* variables and spectra of *Padua-1/7* establish a firm NGC6752 membership.

The origin of the *Padua* variability is unlikely due to some peculiar evolutionary scenarios (e.g. Late Thermal Pulses[19,20]). Indeed, the estimated temperature evolution of *Padua-1*, as due to the $u_{SDSS} - r_{SDSS}$ colour transition in the arc of six years, is $\lesssim 200\,\mathrm{K}$. This is *too slow* for "born again" scenarios involving *rapid* evolution lasting *only* for decades. An additional piece of evidence supporting this conclusion is found when reviewing the position of these long-term EHB variables in color-magnitude diagrams collected decades ago. Identification of Padua-1/2 and 5 in the 1980 B/V photographic plates[21] still reflected typical EHB colors/luminosities. We also exclude the possibility that *Padua-1* variability is due to pulsation, at any short-term regime. In particular, we preclude scenarios like *Blue Large-Amplitude Pulsator* (BLAP[22]: hot sdB showing RR Lyrae-like variability with $\sim 20-40$ minute periods). In this regard, we availed $\sim 3.5\,\mathrm{hours}$ of continuous UltraCAM[23] 20_{sec} u_{SDSS} filter fast-photometry (programme 0103.D-0158, P.I. L. Monaco). Periodogram analysis of the same ultraviolet data showed no significant peaks for pressure-mode oscillations between $100 - 300\,\mathrm{seconds}$.

A close-binary origin is also unlikely. Six spectra of *Padua-1* were collected on the night of November 23rd 2018 at the Low Dispersion Survey Spectrograph (LDSS-3), mounted at the Magellan Clay telescope (Chile). The VPH-Blue grism provided a wavelength coverage between $\sim 3800 - 6200\,\mathrm{\AA}$ and a resolution of ~ 1900. The $6 \times 600_{sec}$ successive spectra were reduced as in Methods 2. These provided a radial velocity RMS of $\sim 11\,\mathrm{km/s}$ with respect to the estimated $\sim 13\,\mathrm{km/s}$ error on single

measurements, suggesting that *Padua-1* is *unlikely* a member of a very-close binary. Similarly, the 6 FLAMES spectra of *Padua-7* (presented in Methods 2) collected over a period of 8 days provided a radial velocity RMS of ~ 4 km/s, very close to the ~ 3 km/s associated error for a given measurement. Combined, the *Padua-1/7* radial velocity monitoring disfavour close-binary systems up to periods of few days. One last piece of evidence arguing against a possible binary origin is found in the estimated energetics of the Padua-1 superflare (10^{39-40} erg). Such levels are much higher than those typically occurring in WD/M-type binary systems[24] (where the flaring event has been associated to an active/cool M-type dwarf). Indeed, had the *Padua-1* superflare been due to a hidden faint/cool K/M-type companion the flare energy would have been orders of magnitudes higher than the strongest flares ever measured in *isolated* K/M-type dwarfs[25]. In conclusion, the *Padua* variables are not pulsators nor members of binary systems.

Granted the above, there is a notable similarity of the form of the *Padua-1* superflare with the occurrence[26,28] of similar outbursts in cool ($T_{eff} \sim 10,900 \pm 300$ K) and pulsating (periods of ~ 1000 seconds) field WDs . With respect to the single/long superflare event in *Padua-1*, the outbursts in these cool/pulsating WDs display[27] a very high re-occurrence frequency of once every ~ 5 days, a short average duration of ~ 12 hours, a slightly higher amplitudes $\sim 10\%$, and much lower energetics $\sim 10^{33}$ erg. Despite these difference, it is interesting to note the very restricted temperature regime of these outbursting WDs (basically coinciding with the G-jump[29]) and its coincidence with the onset of superficial convection by the Hydrogen convection zone (sought[27] to drive the gravity-mode pulsation). In particular, the outbursts are modeled as a "*temporary, rapid re-assignment of kinetic energy away from pulsation*[26]". In this regard, we note that the same scenario we use to explain the occurrence of EHBs' magnetic spots also accommodates for the occurrence of *Padua-1*. In particular, it envisages a "build-up of magnetic energy" but within the hotter sub-surface HeIICZ or in the radiative layer above it[3]. Thus, the "turbulent" effects of the HeIICZ and HCZ, both being so close to the surface (or actually onsetting convective photospheres as in the WDs pulsators) bring about an interesting EHB/WD parallelism. However, the UltraCAM fast photometry of *Padua-1* did not reveal any significant pulsation signature, marking a clear difference with the outbursting/pulsating WDs at $T_{eff} \sim 10,900 \pm 300$ K. Future observational/theoretical investigations are needed to shed more light on the occurrence of outbursting/flaring events and the role played by the surface/sub-surface Hydrogen/Helium convective layers.

α^2 **CVn/Magnetism in Galactic Field sdBs:** One might wonder why the EHB spot-induced α^2 CVn rotational variability in GCs has not been detected in the Galactic field sdB counterparts, despite the latter being subject of many surveys. In principle, there is no *a priori* reason for which the EHB field-counterparts *should not* display α^2 CVn variability. Indeed, Galactic field sdB (as GC EHB stars) display the same complex enhancement/depletion chemical anomalies attributed to diffusion effects (i.e. chemically peculiar). Hence, we argue that the apparent lack of α^2 CVn variability detection in field sdB is likely due to it being hampered by, other, specific sdB properties. For example, with a frequency of $\sim 50\%$[30], the preferential sdB close-binary evolution of the two components is likely to dominate/conceal the lower-amplitude α^2 CVn variability in the light curves. Moreover, eventual tidally-locked components (stellar rotation is synchronised with the orbital period) is likely to induce faster-rotation of the components and shift the α^2 CVn variability to shorter-periods. Overall, and with respect to EHBs in GCs, the sdBs' much-higher binary fraction, their significantly-lower age and relatively-higher metallicity[31] (the latter likely implying differences in stellar spots sizes and

contrast[32]) are all factors possibly contributing in smearing the signature of α^2 CVn variability in field sdBs.

In this regard, space-based surveys probe the millimagnitude variability regime and allow deeper examination of eventual detection of α^2 CVn variability in field sdBs. We bring to the attention the case of CD-38 222, holding TESS[33] serial number 118327563. The physical parameters[25,34] of this star ($T_{eff} \simeq 26,300\,\text{K}$, $log\,L/L_\odot = 1.42$ and $log\,g = 5.5$) place it perfectly in the EHB segment, just hotter than the M-jump. CD-38 222, one of the few cases of an apparently[35] *single* sdB. It was concluded[25] to display rotational variability with a period of ~ 0.229 days and semi-amplitude of less than one part per thousand (as seen in the upper panel in Supplementary Fig. 6. Such low-levels of variability amplitudes can easily escape detection in ground-based surveys[32,36], but are perfectly in line with *all* sdBs being chemically peculiar, easily accommodating for the presence of superficial inhomogeneities upon their surface, i.e. spots. Indeed, CD-38 222 is the *first[35]* Galactic field sdB showing *Helium vertical-stratification* (which could be modeled[14] as due to Helium-enhancement at the magnetic poles of a Helium-spot, as explained in Supplementary Information 1). The extremely low-amplitude variability detected in CD-38 222, *possibly* a representative of the $\lesssim 20\%$ minority of *single* sdB stars, is probably suggestive of how/why α^2 CVn variability is apparently lacking among field sdBs.

While definitive evidence indicates that CD-38 222 is not a member of a *close-binary* system, there remains a suggestion[36] it might hide a faint K-type companion in a wide-orbit. However, the high energetics of the superflare in CD-38 222 makes it unlikely that the K-type dwarf is the source of the superflare. Indeed, a hypothetical superflare in the K-type dwarf would imply energetics that are orders of magnitude stronger than those typically measured in isolated flaring K/M-type dwarfs[25]. One final piece of evidence unambiguously supporting the *single-sdB* star nature of CD-38 222 is provided when assuming that the ~ 0.22-day light modulation is due to a rotating spot on the $\sim 0.25\,\text{R}_\odot$ (as inferred from its luminosity/temperature). This delivers a rotational velocity of $\sim 55.5\,\text{km/s}$ in excellent agreement (considering all sources uncertainties) with two estimates of the projected rotational velocities of ~ 48.0 and $\sim 58.0\,\text{km/s}$, respectively derived from metal and Helium line profiles[36].

CD-38 222 is perhaps a unique case of an sdB also showing the presence of a superflare[25] event (releasing up to $\sim 10^{35}\,\text{erg}$, thousand times more energetic than those occurring in the Sun). This superflare event necessarily implies the presence of an underlying magnetic field in the sdB. Most interestingly, the magnetic field of CD-38 222 has been investigated twice[34,37] only to conclude it being confined to below $\sim 400\,\text{Gauss}$, i.e. below the significance detection-levels of current top-level instrumentations. Thus, by all means, the presence of a low-intensity magnetic field in CD-38 222 *is* certain, regardless of it being detected or not. This is particularly relevant as it lends support to our conclusions on the detected EHB variability and therein presence of similar, low-intensity, magnetic fields. In conclusion, CD-38 222 paves the way for the detection of spot-induced α^2 CVn variability and superflare events in field sdBs, as we have established here for GCs EHBs. Clearly, statistically significant sdB/EHB samples are mandatory before a comparative analysis (e.g. differences in flare duration/energies and α^2 CVn periods/amplitudes) can be performed.

It is probably too early to evaluate the wider implications of universal magnetism among GCs' EHBs and field's sdBs. This is specially true considering that the matrix managing the formation of EHBs in GCs is rather complex (interplay between cluster's age, cluster's central concentration, Helium-enrichment and mixing, CNO abundance, stellar rotation, and extreme mass-loss) whereas that gov-

erning the sdBs formation is restricted to *binarity* ($\sim 80\%$ are *currently* in binaries while the remaining $\sim 20\%$ are merger products of *past* binary evolution). One notes that binary evolution is not even considered as a formation channel for EHBs in GCs. In this regard, we cannot help but notice that the only sdB star showing both α^2 CVn variability and superflare event (and very likely a *single-star*) is also known for a relatively high rotation velocity. The latter is often used as a signature of merger events, and overall there are suggestions that stellar mergers are likely related to a strong magnetic phenomenon[38]. This opens to the remote (but not to be excluded) possibility that the *entirety* of EHBs in GCs can be by-products of stellar mergers. Interestingly, this possibility has been validated by simulations[39] showing that the (WD/WD) merger channel - in stellar systems older than ~ 8 Gyr - is expected to dominate the (Roche lobe overflow and the common-envelope) channels and form more than $\geq 50\%$ of the total EHB fraction in a typical GC. In this regard, the rather high stellar density in GCs (*continuously* favouring encounters/mergers) and the fact that the EHB stars share basically the same distance/reddening/metallicity (i.e. reducing to the minimum temperature/gravity uncertainties) provide the ideal benchmark where one can identify merger-products among EHB stars. Unfortunately, the homogeneous properties of EHBs *currently* show no evidence of any discernible outliers (e.g. larger masses, faster rotation, brighter luminosities, or peculiar red-excess) enabling one to pinpoint a merger by-product in EHBs samples. Ultimately, the merger scenario is left unverified.

α^2 **CVn/Magnetism in Galactic Field WDs:** Despite the common use of WDs as photometric/spectroscopic standards, reports of the presence of stellar spots and related variability date back to the seventies[40,41]. Nowadays, frequent detection of both bright/dark spot-induced photometric variability (on hours-to-day timescales) is reflecting considerably large frequencies ($\sim 50\%$[42] and $\sim 67\%$[43]). Focusing our attention on hot WDs (close to our $\sim 20,000 - 30,000$ K EHB variability regime) we recall WDs characterised by Hydrogen/Helium dominated atmospheres (i.e. DA with $T_{eff} \geq 13,000$ K and DB with $23,000 \leq T_{eff} \leq 28,000$ K, respectively) are both expected to display *fully-radiative* envelopes (as do our EHBs, field B-type and B_P stars). Invoking stellar-spots for cooler WDs with convective atmospheres[44] is, relatively, an easy task (i.e. the hypothesised magnetic fields would inhibit surface convection and naturally form a cooler/darker spot, as is in our Sun). On the other hand, the origin of the photometric variability of hotter/radiative WDs (e.g. LB8915, PG165+441, GD 394 and other 5 cases[42]) remains a mystery[43]. Indeed, conventional (Sun-like) spots cannot be invoked nor formed upon such hot/radiative-enveloped WDs, and magnetic fields (whenever estimated/detected) are apparently not sufficiently strong-enough (at least in the WDs nomenclature) to introduce measurable photometric variability. The case of the $\sim 35,000 - 39,000$ K, Hydrogen-rich, GD 394 is particularly emblematic. Given its apparently single-star status[45] and estimated upper-limit $\sim 12,000$ Gauss magnetic field (would be considered a rather *extremely-weak* field in the WDs context), it is utterly hard to explain its remarkable Far-Ultraviolet, single-wave, variability with ~ 1.15 day period and $\sim 25\%$ amplitude variations. However, its atmosphere is almost certainly radiative and, not-surprisingly, the most likely scenario for its Far-UV variability is one envisaging inhomogeneous surface abundance distribution of metals[45] (aka Far-UV dark/circular spot). This, in principle, is accommodated for by invoking the presence of a, weak, magnetic field.

Many scenarios are put forward to explain the WDs variability[42] and, leaving aside the obvious ones arising due to binary evolution (e.g. transit, beaming, reflection and thermal emission from a close-companion) it all comes down to different shades of a single scenario that combines the WD rotation with "non-uniform surface emission"[42]. In particular, it is interesting to note how the alleged

WDs *surface inhomogeneities* remain the common, fundamental ingredient of apparently "different" modelings[42]; these being cool/dark magnetic spots, hot/bright spots formed due to accretion of ISM material, magnetic dichroism, and most interestingly, non-uniform Far-UV line opacity absorption resulting in optical/near-IR fluorescence. Indeed, the latter scenario was concluded[42] to be the only one that is applicable/viable to *all cases* of variability among WDs (regardless of their envelope structure), and not surprisingly its fundamentals *reflect* what we assume to be the definition of a "magnetic spot" in EHBs. In this regard, the scenario hypothesised for our EHBs (*weak* magnetic fields that do not introduce Zeeman splitting and yet reach the stellar radiative surface) are likely to afflict the temperature of the WD *radiative photosphere* and trigger magnetic spots. In particular, since the optical depth of the WD/EHB photosphere is expectedly *lower* in the magnetic spot surrounding (as due to the contribution of magnetic pressure) it provides a deeper glimpse of the *hotter* stellar interior (i.e. hot/bright magnetic spot)[3].
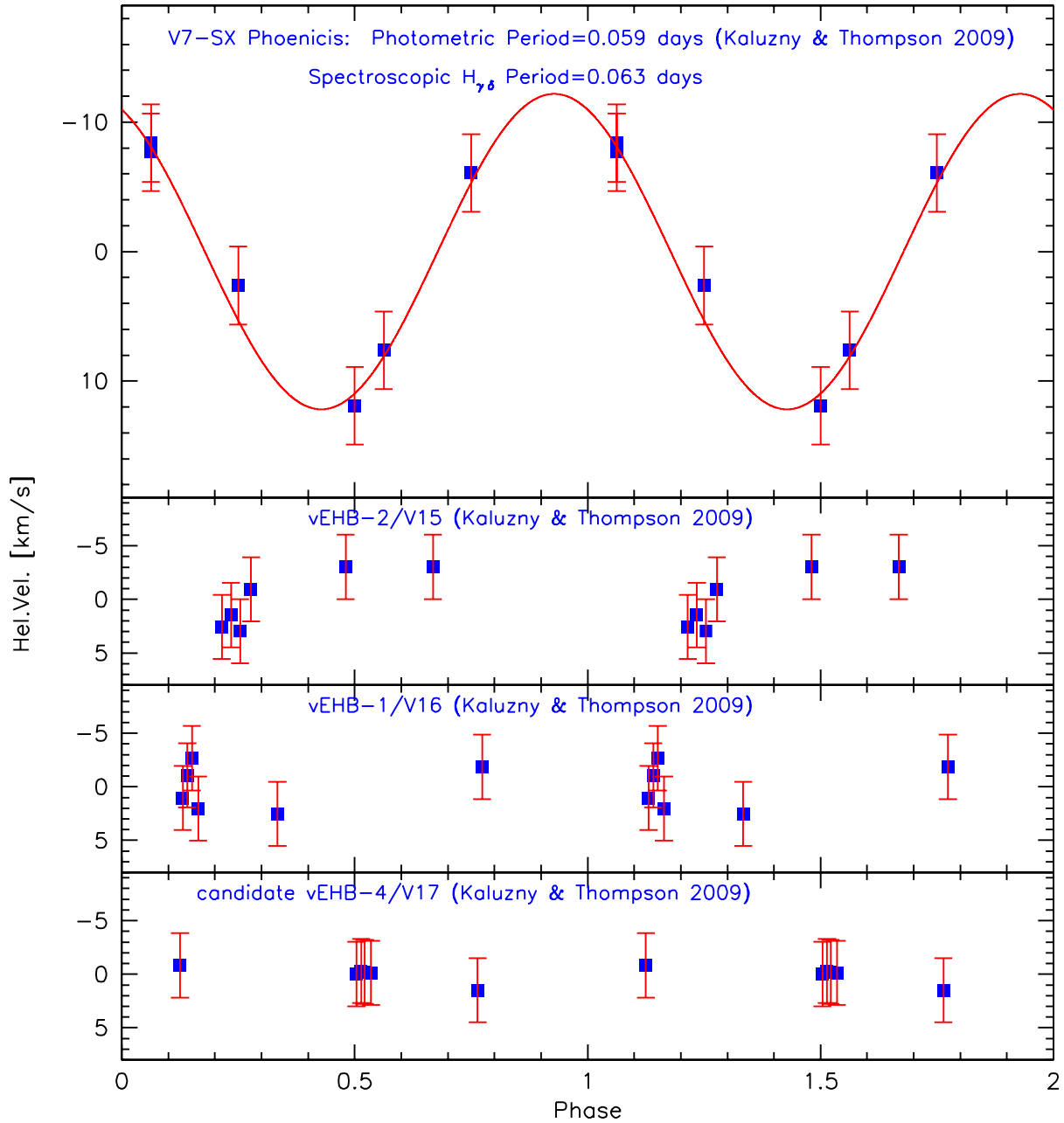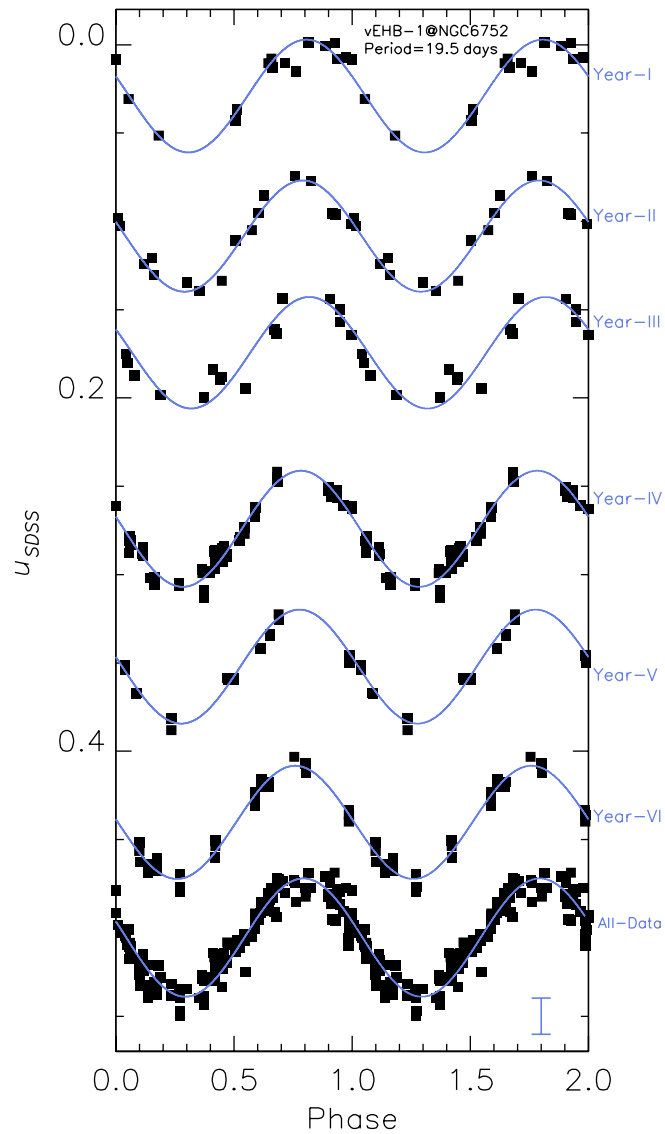
Supplementary Figures
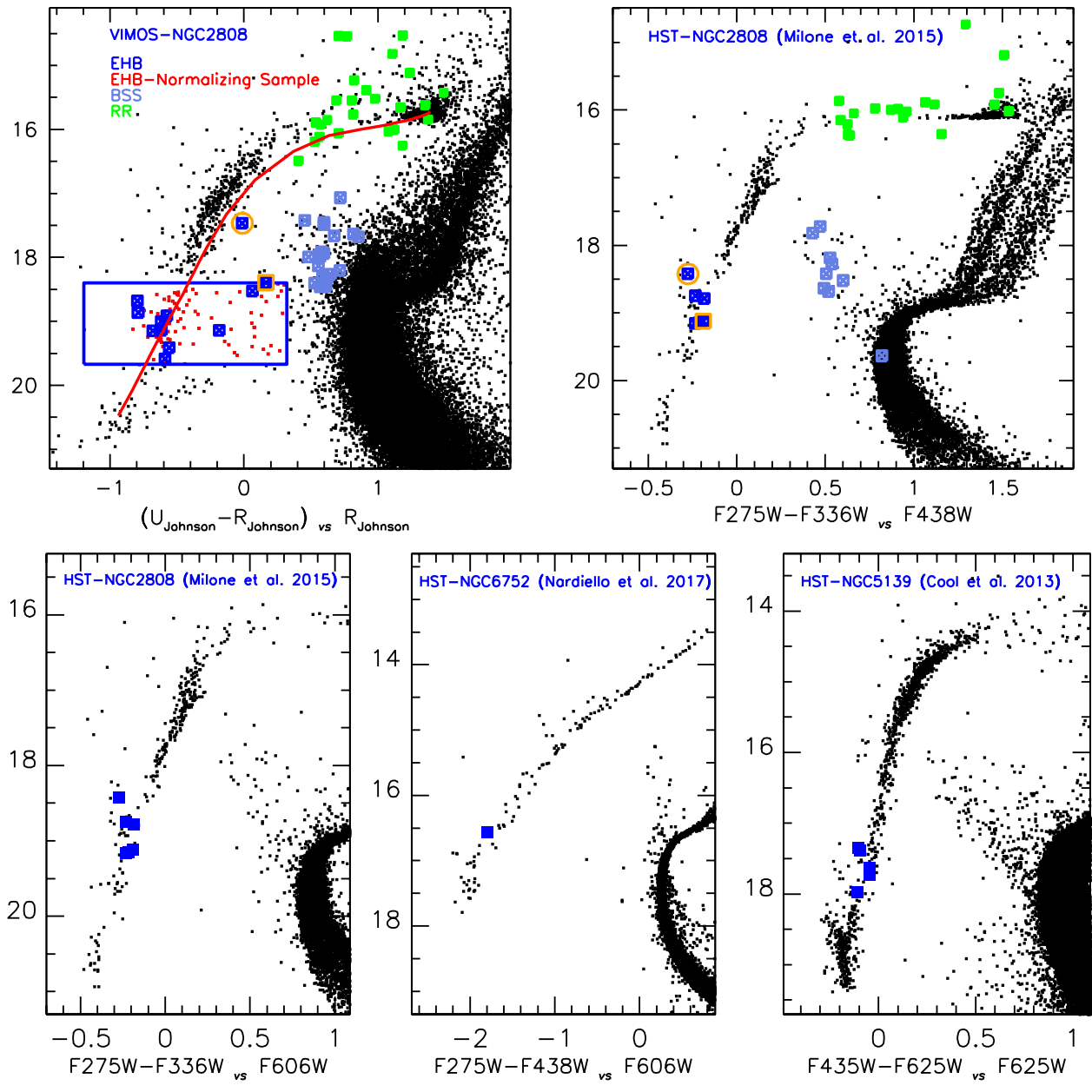
Supplementary Figure 1: Estimating the EHB variable frequency. Upper-left panel displays our NGC2808 VIMOS diagram highlighting all identified variables, the box delimits the EHB sample used to normalise the EHB variables frequency while a ZAHB model is used to confirm the EHB variables temperature range ($\sim 17,500-24,500$ K). The two EHB variables with open orange symbols are *confirmed* EHB stars, as identified in the higher resolution HST catalog (upper-right panel). Lower panels show the position of all EHB variables identified in HST diagrams.
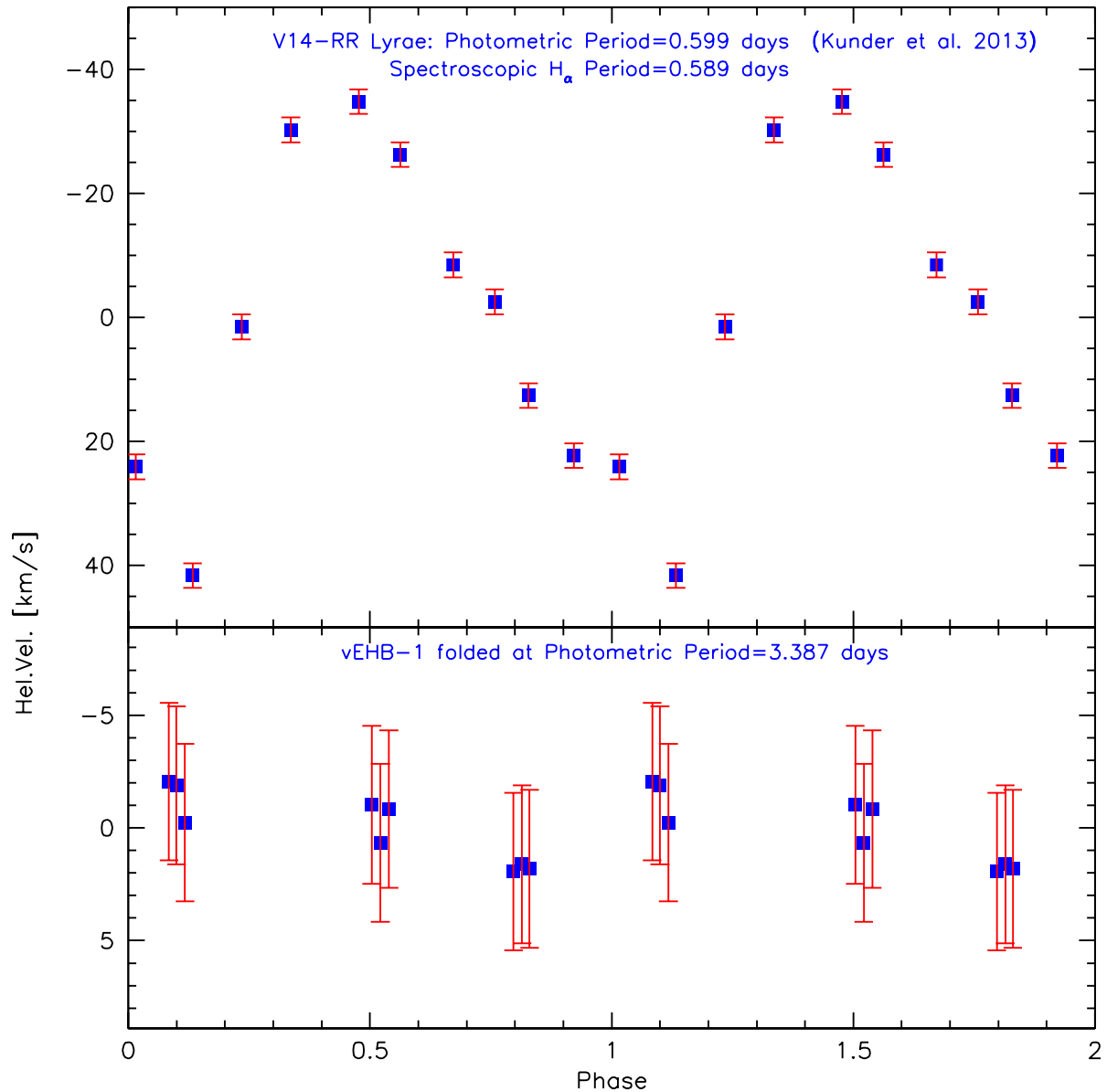
Supplementary Figure 2: No binarity signature detected in the NGC2808 vEHB-1 variable. Upper panel displays the phased H$_\alpha$ radial velocity curve of a *comparison* RR Lyrae star proving a successful detection of velocity variations in the data-set. The lower panel displays the velocity curve of our photometric variable vEHB-1 present in the same data-set. The error bars display the $1 - \sigma$ error (~ 3.5 km/s) estimated at the vEHB-1 luminosity. No significant velocity variations for vEHB-1 are observed. For clarity, the NGC2808 average radial velocity has been subtracted.

Supplementary Figure 3: No binarity signature detected in the NGC6752 vEHB-1/2 variables. Upper panel displays the phased $H_{\gamma\delta}$ radial velocity curve of a *comparison* SX Phoenicis star[46] proving a successful detection of velocity variations in the data-set. The lower panels display the velocity curves of the 2 EHB photometric variables (and the candidate EHB photometric[46] variable vEHB-4/V17) present in the same data-set. The error bars display the $1 - \sigma$ error ($\sim 3.0\,\mathrm{km/s}$) estimated at the vEHB-1 luminosity. No significant velocity variations for the vEHB-1/2 are observed. For clarity, the NGC6752 average radial velocity has been subtracted.

Supplementary Figure 4: The long-term stable variability of vEHB-1 in NGC6752. Bottom plot shows *all* the u_{SDSS} OmegaCAM measurements of vEHB-1 collected over a six-year period. The upper plots show the phased light curves sub-divided over six years. A typical $1 - \sigma$ photometric error bar is plotted. The solid light-blue line is the best fitting model (Period$\simeq$ 19.5 days) calculated using the six years' measurements.
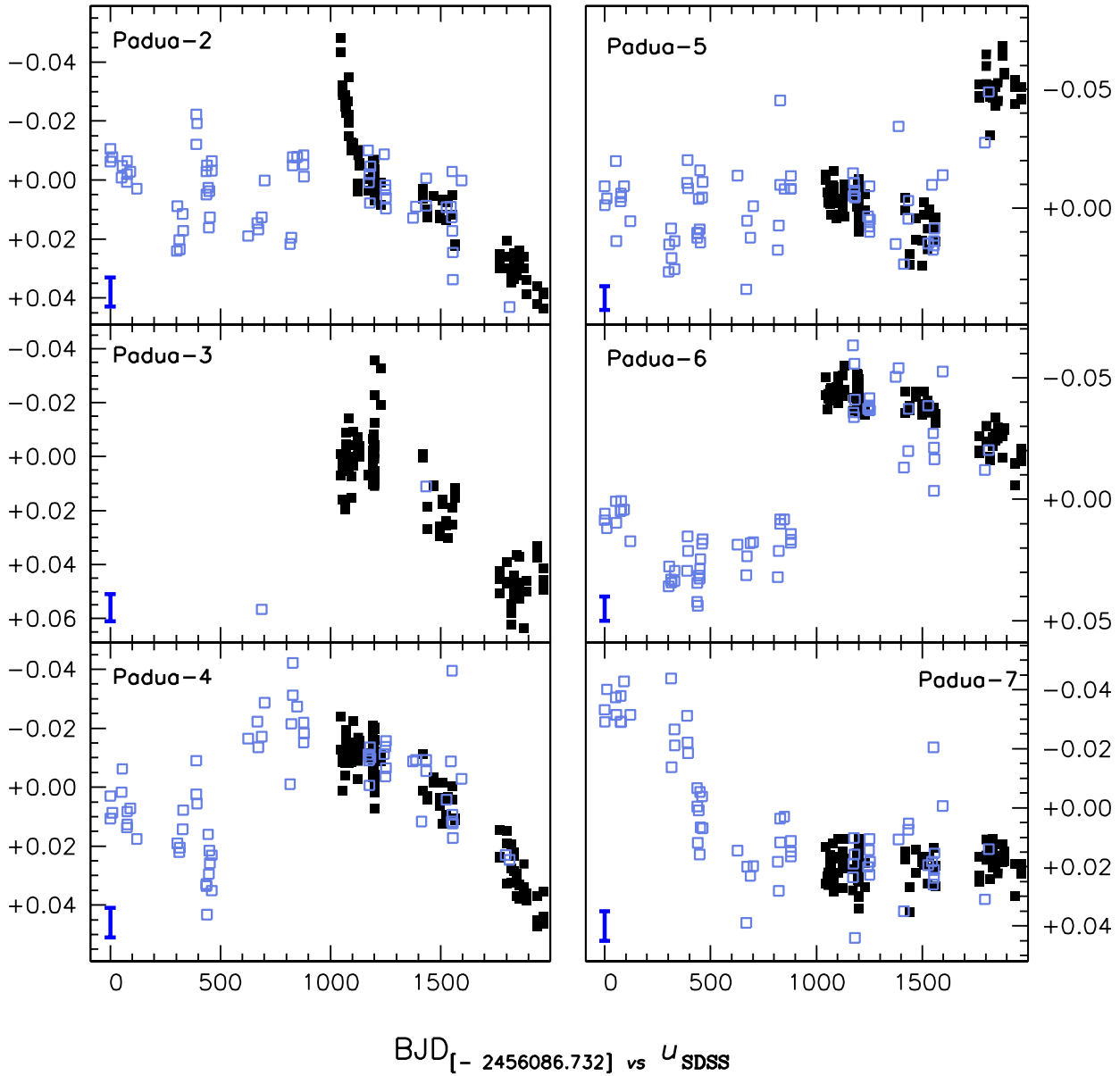
Supplementary Figure 5: The aperiodic long-term *Padua* variables in NGC6752. Light blue squares display the six-year archival OmegaCAM@VST data, while black squares display those originating from our three-year monitoring. A typical $1 - \sigma$ photometric error bar is plotted. The *Padua-2* mini-burst is incomplete but discernible.
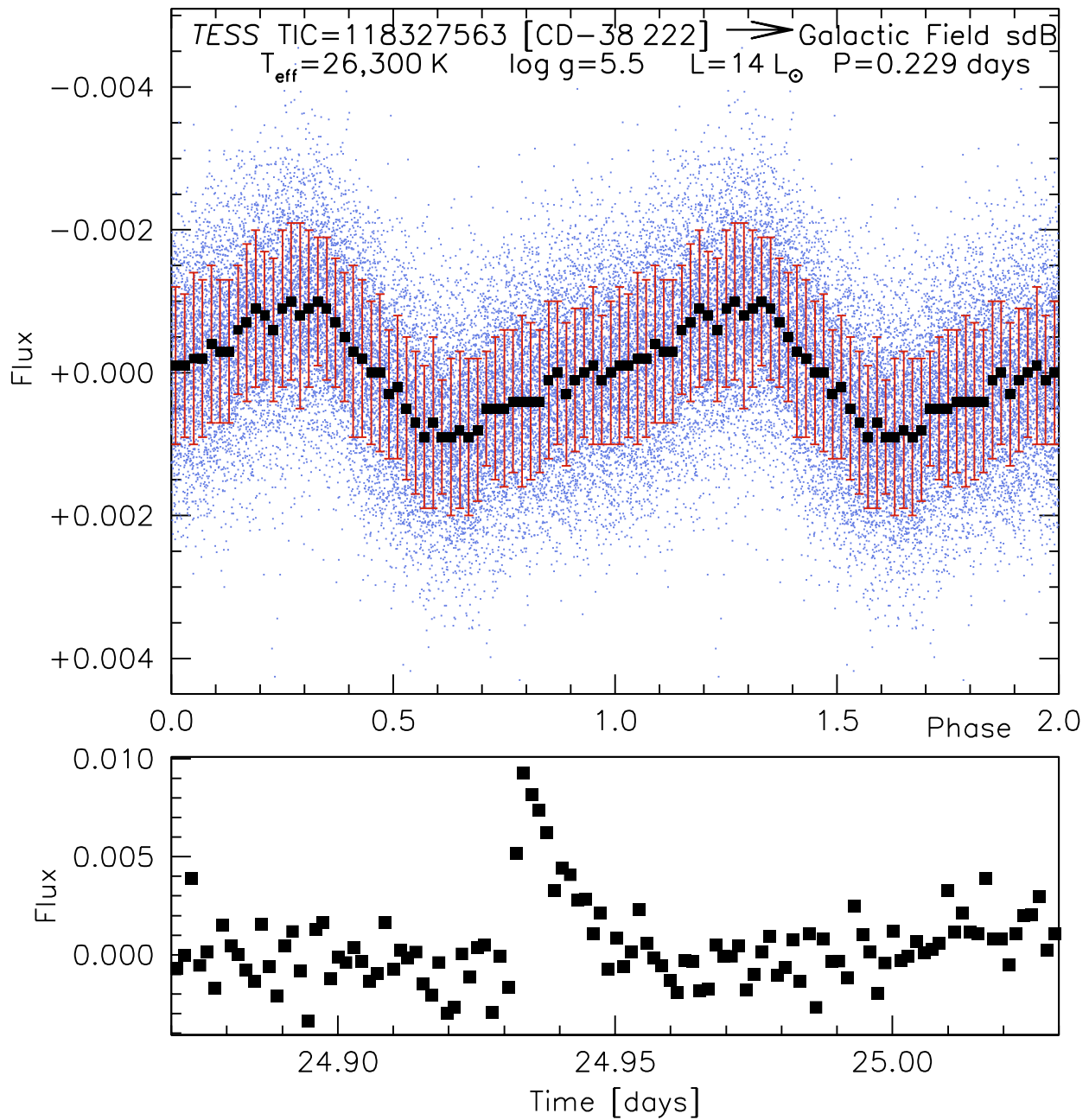
Supplementary Figure 6: Rotational variability and superflare event in a Galactic field sdB. Upper panel displays the folded TESS light curve of a Galactic field sdB showing α^2 CVn spot-induced variability. Filled squares are the $2.5 - \sigma$ clipped median values every 300 data-points, while the error bars reflect the $1 - \sigma$ rms of the clipped Flux values. Lower panel proves the occurrence of an energetic ($\sim 10^{35}$ erg) super-flare event in this field sdB. Both phenomenon necessitate the presence of magnetic fields.

1. Strassmeier, K. G. Starspots. *Astron. Astrophys. Rev.* **17**, 251-308 (2009).

2. Recio-Blanco, A., Piotto, G., Aparicio, A., & Renzini, A. Rotation of Hot Horizontal-Branch Stars in the Globular Clusters NGC 1904, NGC 2808, NGC 6093, and NGC 7078. *Astrophys. J. Lett.* **572**, L71-L74 (2002).

3. Cantiello, M., & Braithwaite, J. Envelope Convection, Surface Magnetism, and Spots in A and Late B-type Stars. *Astrophys. J.* **883**, 106 (2019).

4. Brown, T. M., et al. The Hubble Space Telescope UV Legacy Survey of Galactic Globular Clusters. VII. Implications from the Nearly Universal Nature of Horizontal Branch Discontinuities. *Astrophys. J.* **822**, 44 (2016).

5. Groth, H. G., Kudritzki, R. P., & Heber, U. Photospheric convection zones and evolution of subluminous OB-stars. *Astron. Astrophys.* **152**, 107-116 (1985).

6. Michaud, G., Richer, J., & Richard, O. Horizontal branch evolution, metallicity, and sdB stars. *Astron. Astrophys.* **529**, A60 (2011).

7. Moni Bidin, C., et al. Spectroscopy of horizontal branch stars in ω Centauri⋆. *Astron. Astrophys.* **547**, A109 (2012).

8. Unglaub, K. Mass-loss and diffusion in subdwarf B stars and hot white dwarfs: do weak winds exist?. *Astron. Astrophys.* **486**, 923-940 (2008).

9. Babel, J. The fading of radiatively driven winds in B stars. *Astron. Astrophys.* **309**, 867-878 (1996).

10. Eastman, J., Gaudi, B. S., & Agol, E. EXOFAST: A Fast Exoplanetary Fitting Suite in IDL. *Publ. Astron. Soc. Pac.* **125**, 83 (2013).

11. Montalto, M., et al. Improvements on analytic modelling of stellar spots. *Mon. Not. R. Astron. Soc.* **444**, 1721-1728 (2014).

12. Panja, M., Cameron, R., & Solanki, S. K. 3D Radiative MHD simulations of starspots. arXiv e-prints arXiv:2003.09656 (2020).

13. Stibbs, D. W. N. A study of the spectrum and magnetic variable star HD 125248. *Mon. Not. R. Astron. Soc.* **110**, 395 (1950).

14. Shavrina, A. V., et al. Spots structure and stratification of helium and silicon in the atmosphere of He-weak star HD 21699. *Mon. Not. R. Astron. Soc.* **401**, 1882-1888 (2010).

15. Stift, M. J. A non-axisymmetric rigid rotator model for magnetic stars.. *Mon. Not. R. Astron. Soc.* **172**, 133-139 (1975).

16. Glagolevskij, Y. V., & Chuntonov, G. A. Composite model for the magnetic field of HD 21699. *Astrophys.* **50**, 362-371 (2007).

17. Krtička, J., Mikulášek, Z., Zverko, J., & Žižńovský, J. The light variability of the helium strong star HD 37776 as a result of its inhomogeneous elemental surface distribution. *Astron. Astrophys.* **470**, 1089-1098 (2007).

18. Kawka, A. Clues to the origin and properties of magnetic white dwarfs. arXiv e-prints arXiv:2001.10672 (2020).

19. Schoenberner, D. Asymptotic giant branch evolution with steady mass loss.. *Astron. Astrophys.* **79**, 108-114 (1979).

20. Iben, I. On the frequency of planetary nebula nuclei powered by helium burningand on the frequency of white dwarfs with hydrogen-deficient atmospheres.. *Astrophys. J.* **277**, 333-354 (1984).

21. Buonanno, R., et al. The giant, asymptotic and horizontal branches of globular clusters. III. Photographic photometry of NGC 6752.. *Astron. Astrophys. Suppl.* **66**, 79-109 (1986).

22. Pietrukowicz, P., et al. Blue large-amplitude pulsators as a new class of variable stars. Nature Astronomy **1**, 0166 (2017).

23. Dhillon, V. S., et al. ULTRACAM: an ultrafast, triple-beam CCD camera for high-speed astrophysics. *Mon. Not. R. Astron. Soc.* **378**, 825-840 (2007).

24. Østensen, R. H., et al. First Kepler results on compact pulsators - I. Survey target selection and the first pulsators. *Mon. Not. R. Astron. Soc.* **409**, 1470-1486 (2010).

25. Balona, L. A., et al. Rotational modulation in TESS B stars. *Mon. Not. R. Astron. Soc.* **485**, 3457-3469 (2019).

26. Hermes, J. J., et al. A Second Case of Outbursts in a Pulsating White Dwarf Observed by Kepler. *Astrophys. J. Lett.* **810**, L5 (2015).

27. Bell, K. J., et al. The First Six Outbursting Cool DA White Dwarf Pulsators. In *Proceedings of the 20st European Workshop on White Dwarfs*, **509**, 303 (2017).

28. Bell, K. J., et al. KIC 4552982: Outbursts and Asteroseismology from the Longest Pseudo-continuous Light Curve of a ZZ Ceti. *Astrophys. J.* **809**, 14 (2015).

29. Grundahl, F., Catelan, M., Landsman, W. B., Stetson, P. B., & Andersen, M. I. Hot Horizontal-Branch Stars: The Ubiquitous Nature of the "Jump" in Strömgren u, Low Gravities, and the Role of Radiative Levitation of Metals. *Astrophys. J.* **524**, 242-261 (1999).

30. Deca, J., et al. PG 1018-047: the longest period subdwarf B binary. *Mon. Not. R. Astron. Soc.* **421**, 2798-2808 (2012).

31. Latour, M., et al. A Helium-Carbon Correlation on the Extreme Horizontal Branch in ω Centauri. *Astrophys. J.* **795**, 106 (2014).

32. Paunzen, E., et al. Search for stellar spots in field blue horizontal-branch stars. *Astron. Astrophys.* **622**, A77 (2019).

33. Ricker, G. R., et al. Transiting Exoplanet Survey Satellite (TESS). *Journal of Astronomical Telescopes, Instruments, and Systems* **1**, 014003 (2015).

34. Landstreet, J. D., Bagnulo, S., Fossati, L., Jordan, S., & O'Toole, S. J. The magnetic fields of hot subdwarf stars. *Astron. Astrophys.* **541**, A100 (2012).

35. Schneider, D., Irrgang, A., Heber, U., Nieva, M. F., & Przybilla, N. NLTE spectroscopic analysis of the ^{3}He anomaly in subluminous B-type stars. *Astron. Astrophys.* **618**, A86 (2018).

36. Geier, S., et al. The subdwarf B star SB 290 - A fast rotator on the extreme horizontal branch. *Astron. Astrophys.* **551**, L4 (2013).

37. Bagnulo, S., Fossati, L., Landstreet, J. D., & Izzo, C. The FORS1 catalogue of stellar magnetic field measurements. *Astron. Astrophys.* **583**, A115 (2015).

38. García-Berro, E., et al. Double Degenerate Mergers as Progenitors of High-field Magnetic White Dwarfs. *Astrophys. J.* **749**, 25 (2012).

39. Han, Z. A possible solution for the lack of EHB binaries in globular clusters. *Astron. Astrophys.* **484**, L31-L34 (2008).

40. Landi Degl'Innocenti, E. Are there spots on magnetic white dwarfs? *Astrophys. J.* **209**, 208-213 (1976).

41. Sion, E. M., Schaefer, K. G., Bond, H. E., Saffer, R. A., & Cheng, F. H. Hubble Space Telescope Observations of an Accreted Silicon SPOT on the White Dwarf in V471 Tauri. *Astrophys. J. Lett.* **496**, L29-L32 (1998).

42. Maoz, D., Mazeh, T., & McQuillan, A. Kepler and the seven dwarfs: detection of low-level day-time-scale periodic photometric variations in white dwarfs. *Mon. Not. R. Astron. Soc.* **447**, 1749-1760 (2015).

43. Brinkworth, C. S., Burleigh, M. R., Lawrie, K., Marsh, T. R., & Knigge, C. Measuring the Rotational Periods of Isolated Magnetic White Dwarfs. *Astrophys. J.* **773**, 47 (2013).

44. Kilic, M., et al. A Dark Spot on a Massive White Dwarf. *Astrophys. J. Lett.* **814**, L31 (2015).

45. Dupuis, J., Chayer, P., Vennes, S., Christian, D. J., & Kruk, J. W. Adding More Mysteries to the DA White Dwarf GD 394. *Astrophys. J.* **537**, 977-992 (2000).

46. Kaluzny, J., & Thompson, I. B. Variable Stars in the Globular Cluster NGC 6752. *Acta Astron.* **59**, 273-289 (2009).

47. Momany, Y., et al. A New Feature along the Extended Blue Horizontal Branch of NGC 6752. *Astrophys. J. Lett.* **576**, L65-L68 (2002).

48. Momany, Y., et al. The ubiquitous nature of the horizontal branch second U-jump. A link with the Blue Hook scenario?. *Astron. Astrophys.* **420**, 605-617 (2004).

49. Milone, A. P., et al. The Hubble Space Telescope UV Legacy Survey of Galactic Globular Clusters. III. A Quintuple Stellar Population in NGC 2808. *Astrophys. J.* **808**, 51 (2015).

50. Moni Bidin, C., Villanova, S., Piotto, G., & Momany, Y. A lack of close binaries among hot horizontal branch stars in globular clusters. II. NGC 2808. *Astron. Astrophys.* **528**, A127 (2011).

51. Nardiello, D., et al. The Hubble Space Telescope UV Legacy Survey of Galactic Globular Clusters - XVII. Public Catalogue Release. *Mon. Not. R. Astron. Soc.* **481**, 3382-3393 (2018).

52. Cool, A. M., et al. HST/ACS Imaging of Omega Centauri: Optical Counterparts of Chandra X-Ray Sources. *Astrophys. J.* **763**, 126 (2013).

53. Moehler, S., et al. The hot horizontal-branch stars in ω Centauri. *Astron. Astrophys.* **526**, A136 (2011).

54. Latour, M., Randall, S. K., Calamida, A., Geier, S., & Moehler, S. SHOTGLAS. I. The ultimate spectroscopic census of extreme horizontal branch stars in ω Centauri. *Astron. Astrophys.* **618**, A15 (2018).

Table 1: The measured J2000 coordinates and Johnson-UBV magnitudes of the EHB variables in NGC2808, NGC6752[47] and NGC5139[48], respectively. The last four columns report the distance (in arcmin) from the GC centre, the derived period, the full-amplitude as measured in the ultraviolet-filter ($U_{Johnson}$ for NGC2808 and u_{SDSS} for NGC6752 and NGC5139) and, when available, information regarding their temperature, radial velocity monitoring, and presence in HST catalogs.

ID	Ra	Dec	U	B	V	Dist.[′]	Period [days]	Amp. [U/u]	Notes
vEHB-1	137.9621546	−64.87790004	18.521	19.171	19.164	1.5	3.38683880	0.201	T_{eff} = 20,500 K, No RV variations, HST[49]
vEHB-2	138.0497832	−64.86663111	18.381	18.871	—	1.0	5.47704961	0.181	HST[49]
vEHB-3	137.9542449	−64.83859281	19.000	19.698	19.781	2.0	26.01823489	0.085	
vEHB-4	137.9990148	−64.82868587	18.466	19.043	18.903	2.1	1.97628738	0.074	
vEHB-5	137.9939763	−64.89030570	18.955	19.565	19.337	1.7	3.23990003	0.129	T_{eff} = 17,900 K[50], No RV variations[50]
vEHB-6	137.8985627	−64.82620402	18.857	19.476	19.538	3.6	50.10395158	0.089	
vEHB-7	138.0109231	−64.874611991	17.454	18.008	17.779	0.7	3.02583807	0.082	HST[49]
vEHB-8	137.9761837	−64.85830270	18.075	18.623	18.661	0.9	2.89086189	0.109	HST[49]
vEHB-9	137.9968552	−64.83232443	18.588	19.126	18.817	1.9	6.90595098	0.081	
vEHB-10	138.0230711	−64.89646162	17.888	18.666	18.728	2.0	3.58179363	0.059	
vEHB-11	138.0331348	−64.85209383	18.559	19.028	18.750	0.9	3.19599005	0.091	HST[49]
vEHB-12	137.7036732	−64.85410887	18.340	18.833	19.007	7.8	4.26386105	0.221	
vEHB-13-candidate	138.0365184	−64.851004491	18.055	18.617	18.819	1.0	0.80305948	0.075	HST[49]
vEHB-14-candidate	137.9571663	−64.903780587	18.647	19.177	18.926	2.8	11.37292900	0.043	
vEHB-15-candidate	138.0315200	−64.830937154	18.653	19.363	19.364	2.0	2.32221267	0.041	
vEHB-1/V16	287.7767690177	−59.980062960	15.598	16.404	16.608	1.8	19.54612162	0.079	HST[51], No RV variations
vEHB-2/V15	287.7971182867	−59.995938057	15.444	16.199	16.358	2.6	2.27672174	0.037	No RV variations
Padua-1	287.489983795	−60.031265955	16.174	17.092	17.348	7.4	lpv	<0.1	T_{eff} = 29,800 K, No RV variations
Padua-2	287.686888358	−59.951220918	16.055	16.956	17.191	2.0	lpv	<0.1	
Padua-3	287.698905364	−59.982337781	16.227	16.956	16.923	0.5	lpv	<0.1	
Padua-4	287.678071371	−59.963366804	16.361	17.270	17.501	1.6	lpv	<0.1	
Padua-5	287.652237292	−59.887642791	16.500	17.453	17.664	6.0	lpv	<0.1	
Padua-6	287.658750464	−60.011251791	15.923	16.843	17.054	2.5	lpv	<0.1	
Padua-7	287.628541757	−59.930214607	16.208	17.095	17.280	4.1	lpv	<0.1	No RV variations
vEHB-3-candidate	287.676080625	−60.018833877	15.748	16.495	16.662	2.5	1.855326900	0.043	No RV variations
vEHB-4/V17-candidate	287.766889084	−59.985405659	15.410	15.370	15.311	1.5	3.28778877277	0.031	
vEHB-1	201.745948987	−47.490663552	16.852	17.569	17.631	2.4	11.42978680	0.177	HST[52]
vEHB-2/NV-380	201.594051157	−47.514662905	16.476	17.224	17.249	4.5	7.82858823	0.132	T_{eff} = 28,200 K[53], No RV variations[53] ,HST[52]
vEHB-3/NV-404	201.591343236	−47.434931385	16.569	17.189	17.274	4.8	5.16509016	0.107	HST[52]
vEHB-4	201.859030855	−47.443357761	16.953	17.621	17.671	7.1	4.45548674	0.107	T_{eff} = 24,494 K[54]
vEHB-5	201.759893238	−47.419636276	17.275	18.068	18.104	4.4	2.14022724	0.139	HST[52]
vEHB-6	201.743567846	−47.486164373	16.989	17.742	17.849	2.2	2.06371151	0.099	HST[52]
vEHB-7	201.822724024	−47.463627490	16.831	17.582	17.644	5.4	1.78352993	0.071	T_{eff} = 23,829 K[54]
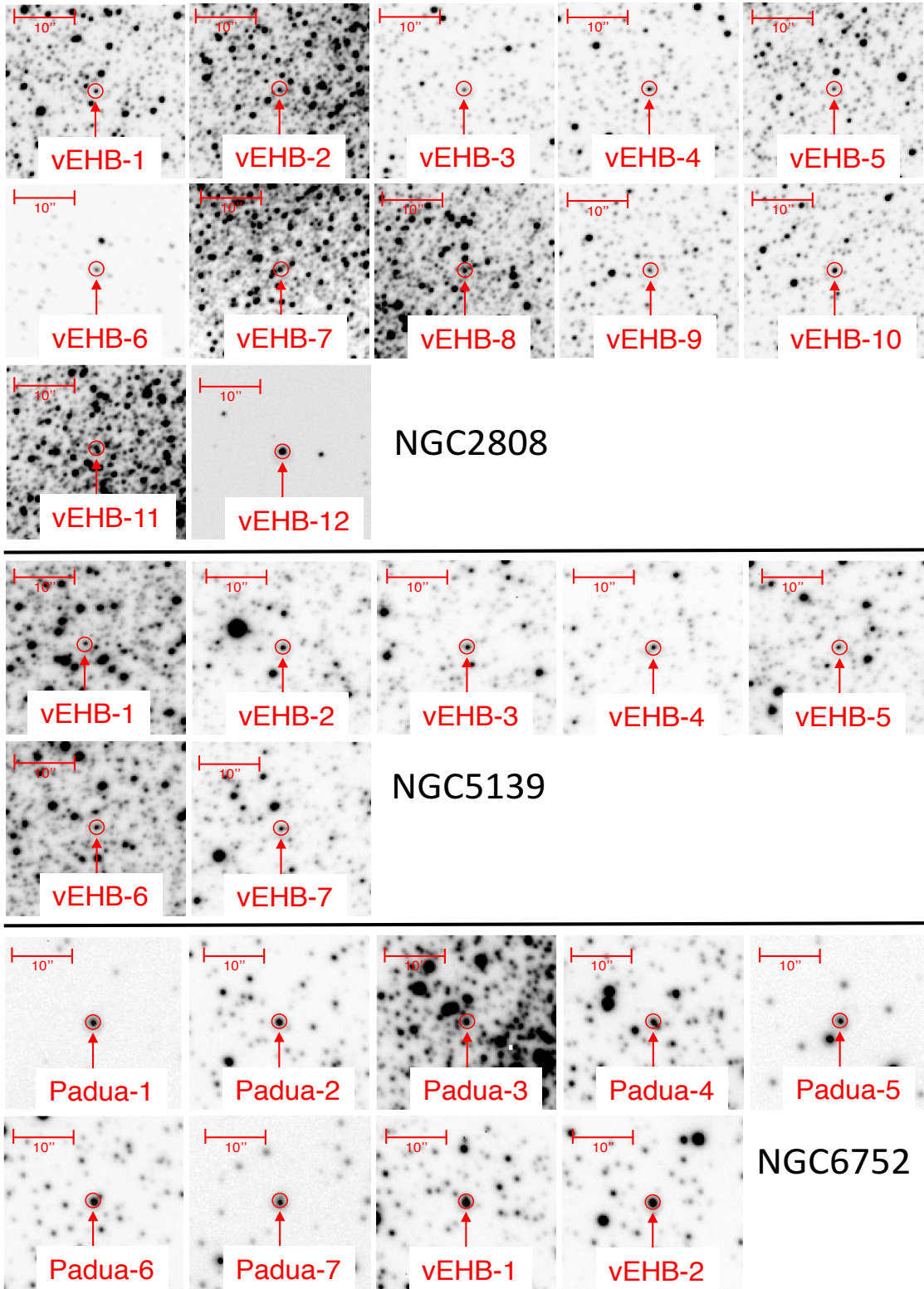
Supplementary Figure 7: Finding charts for our reported EHB and Padua variables. Each chart is 30″ on a side; North is up while East is to the left. The charts are based on our near-ultraviolet Johnson $U_{Johnson}$ filter (NGC2808) and sloan u_{SDSS} filter (NGC6752 and NGC5139) images.